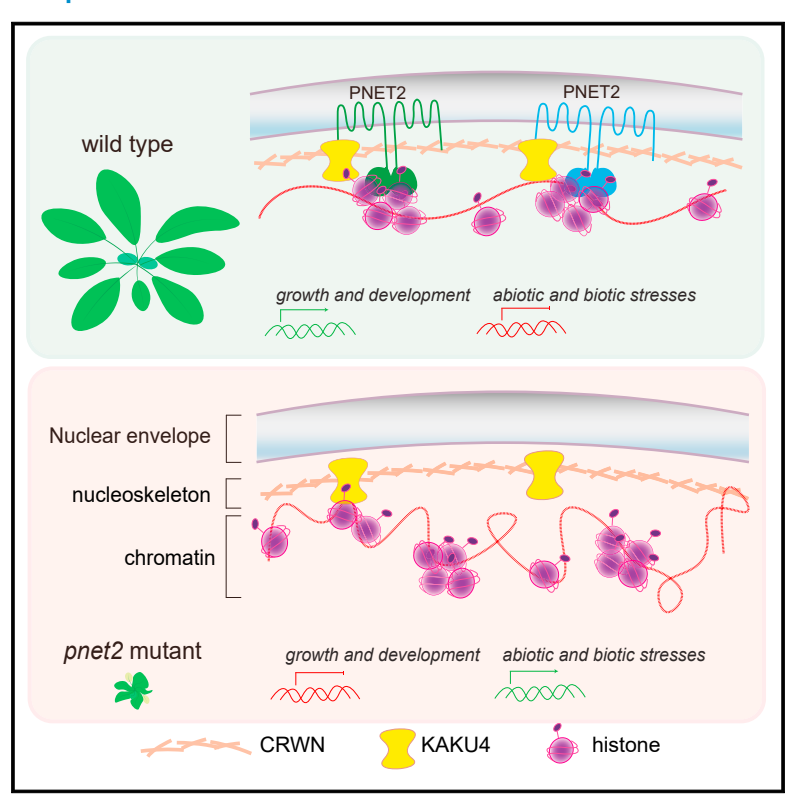
# PNET2 is a component of the plant nuclear lamina and is required for proper genome organization and activity

#### **Graphical abstract**



#### **Authors**

Yu Tang, Qianli Dong, Tianya Wang, Lei Gong, Yangnan Gu

#### Correspondence

guyangnan@berkeley.edu

#### In brief

Tang et al. report that a conserved inner nuclear membrane protein PNET2 is an essential component of the nuclear lamina in plants. PNET2 mediates chromatin tethering to the nuclear periphery and is required to maintain the proper chromatin architecture and transcription programming that balances plant growth and stress responses.

#### **Highlights**

- PNET2 is an inner nuclear membrane protein that binds with nucleoskeleton proteins
- PNET2 associates with nucleosome-enriched chromatin
- Loss of PNET2 restricts growth and activates a wide range of stress responses
- The higher-order chromatin organization is disrupted in the absence of PNET2







#### **Article**

# PNET2 is a component of the plant nuclear lamina and is required for proper genome organization and activity

Yu Tang,<sup>1,2</sup> Qianli Dong,<sup>3</sup> Tianya Wang,<sup>3</sup> Lei Gong,<sup>3</sup> and Yangnan Gu<sup>1,2,4,\*</sup>

#### **SUMMARY**

The interaction between chromatin and the nuclear lamina (NL) is intrinsically important to the establishment of three-dimensional chromatin architecture and spatiotemporal regulation of gene expression. However, critical regulators involved in this process are poorly understood in plants. Here, we report that *Arabidopsis* PNET2 and its two homologs are bona fide inner nuclear membrane proteins and integral components of the NL. PNET2s physically interact with the plant nucleoskeleton and engage nucleosome-enriched chromatin at the nuclear periphery. Loss of all three PNET2s leads to severely disrupted growth and development, concomitant activation of abiotic and biotic stress responses, and ultimate lethality in *Arabidopsis*. The *pent2* triple mutant also displays drastic transcriptome changes accompanied by a globally altered chromatin architecture revealed by HiC analysis. Our study identified PNET2 as an inner nuclear membrane (INM) component of the NL, which associates with chromatin and play a critical role in orchestrating gene expression and chromatin organization in plants.

#### INTRODUCTION

The nuclear envelope (NE) is the hallmark of the eukaryotic cell and is composed of two concentric membranes, the outer nuclear membrane (ONM) that faces the cytoplasm and the inner nuclear membrane (INM) that makes direct contacts with nucleoplasmic contents. Underneath the INM, lamin and lamin-like nucleoskeletal proteins interact with integral INM proteins to form a meshwork structure called nuclear lamina (NL).

Emerging evidence showed that the NL is the primary interacting interface between the INM and the genome and functions as an essential platform for the nonrandom spatial organization of chromatin within the nucleus (Amendola and van Steensel, 2014). The NL-mediated chromatin tethering to the nuclear periphery is tightly regulated during cell development and differentiation and profoundly affects the expression of genes, although the mechanism has not been fully understood (Finlan et al., 2008; Mekhail and Moazed, 2010; Misteli, 2007). In metazoan, the nuclear periphery generally establishes a transcriptionally quiescent environment that is usually associated with heterochromatin and genomic regions with repressed gene expression (Kind and van Steensel, 2010; Reddy et al., 2008; Shevelyov et al., 2009; Towbin et al., 2009), whereas active chromatin is largely distributed in the nuclear interior and nuclear pore regions (Ptak et al., 2014). Similarly, in plants, the nuclear-peripheryanchored chromatin domains were found to be enriched with transposons, inactive protein-coding genes, and repressive histone marks (Bi et al., 2017; Hu et al., 2019). In contrast, active biosynthetic gene clusters locate away from the nuclear periphery in the plant cell (Nützmann et al., 2020), and artificially targeting genes to the nuclear pore complex (NPC) could increase their expression (Smith et al., 2015).

In metazoan, transmembrane proteins localized to the INM have long been shown to selectively interact with chromatin and play a major role in recruiting chromatin to the NE and requlate their activity. LAP2-emerin-Man1 (LEM)-domain-containing protein family represents a prominent example (Brachner and Foisner, 2011). The core feature of the LEM domain is a bi-helical motif of  $\sim$ 40 amino acids that binds to barrier-to-autointegration factor (BAF), a conserved chromatin-associated protein found in all metazoans (Jamin and Wiebe, 2015; Margalit et al., 2005; Zheng et al., 2000). LEM proteins may also bind chromatin independent of BAF because LEM itself is thought to evolve from an ancestral DNA-binding protein and is highly related to the SAFacinus-PIAS (SAP) and helix-extension-helix (HeH)-domain-containing superfamilies, which can directly bind with DNA (Aravind et al., 2002; Brachner and Foisner, 2011; Suzuki et al., 2009). LEM proteins bridge the NE with repressed chromatin (Guelen et al., 2008; Ikegami et al., 2010) and recruit histone deacetylases (e.g., HDAC3) to epigenetically maintain repressed chromatin states (Demmerle et al., 2012; Somech et al., 2005). In yeast, LEM-related proteins are required for NE positioning of



<sup>&</sup>lt;sup>1</sup>Department of Plant and Microbial Biology, University of California, Berkeley, CA 94720, USA

<sup>&</sup>lt;sup>2</sup>Innovative Genomics Institute, University of California, Berkeley, CA 94720, USA

<sup>&</sup>lt;sup>3</sup>Key Laboratory of Molecular Epigenetics of the Ministry of Education (MOE), Northeast Normal University, Changchun 130024, China <sup>4</sup>Lead contact

<sup>\*</sup>Correspondence: guyangnan@berkeley.edu https://doi.org/10.1016/j.devcel.2021.11.002



sub-telomeric loci and ribosomal DNA repeats to repress gene expression and to promote the stability of repetitive sequences, respectively (Grund et al., 2008; Mekhail et al., 2008). Loss of LEM proteins is intimately linked with a myriad of human diseases, including muscular dystrophy, cardiomyopathy, bone density disorders, and cancers (Bione et al., 1994; Brachner and Foisner, 2014; Wong et al., 2014).

Despite the prominent role of LEM proteins in regulating chromatin organization and transcription activity in metazoan, plant genomes do not encode any protein that contains LEM domains. Whether integral INM proteins play a role in chromatin tethering to the NL and how they may affect the chromatin organization and transcription activity are poorly understood in plants.

Here, we identified functionally redundant homologs of plant nuclear envelope transmembrane 2 (PNET2) as bona fide INM proteins and integral components of the NL in Arabidopsis. We found that PNET2 proteins physically interact with nucleoskeletal protein CRWN1 (CROWDED NUCLEI 1) and engage nucleosomes at the nuclear periphery together with KAKU4. Loss of PNET2 genes in Arabidopsis resulted in severely restricted growth and drastically altered transcriptome landscape that displays inhibition of cell division and induction of a wide range of abiotic and biotic stress responses. Further analysis of the pnet2 mutant using high-throughput chromatin conformation capture (HiC) revealed significant changes in the spatial organization of chromatin compared with wild-type plants, including enhanced short-distance gene-gene interaction, reduced long-distance intra- and inter-chromosomal interactions, and potential alterations in euchromatic and heterochromatic status. We propose that PNET2 proteins function as essential components of the plant NL and intimately associate with nucleosome-enriched chromatin at the NE to contribute to the proper maintenance of genome architecture and transcriptome programing in plants.

#### **RESULTS**

#### Identification of PNET2\_A by proximity labeling proteomics using MAN1 as bait

To identify plant INM proteins that are potentially involved in engaging chromatin with the NL, we started with characterizing the Arabidopsis homolog of MAN1, a conserved INM protein found across eukaryotes (Brachner and Foisner, 2011). Unlike in animals and yeast, the Arabidopsis MAN1 gene (At5g46560) encodes a protein that lacks a LEM domain in its N terminus. Nonetheless, AtMAN1 contains two transmembrane (TM) helices and a conserved C-terminal MSC (MAN1/SRC1p/C-terminal motif) domain, which has been shown to mediate DNA binding in humans (Caputo et al., 2006), suggesting that the plant MAN1 protein may retain a function in the INM. Indeed, we found that the yellow fluorescence protein (YFP) tagged AtMAN1 fusion protein specifically localizes to the nuclear periphery when stably expressed in transgenic Arabidopsis seedlings (Figure S1A). However, we found that the T-DNA knockout man1 mutant (Salk\_024888) did not exhibit discernible phenotypes compared with WT plants (Figures S1B and S1C). In contrast, mutations in the majority of animal LEM genes involved in chromatin tethering cause various diseases (Wong et al., 2014), and in particular, loss of MAN1 leads to early embryonic lethality in mice (Cohen et al., 2007; Ishimura et al., 2006). These results suggest that plant MAN1 may function as a conserved INM protein that associates with chromatin but argue that other INM proteins may also contribute to chromatin tethering in plants.

To search for INM proteins that are potentially involved in chromatin association in plants, we fused AtMAN1 with the promiscuous biotin ligase BioID2 (Kim et al., 2016), which enables proximity-dependent protein biotinylation and subsequent mass spectrometry (MS) identification of proteins that are close to MAN1 and MAN1-associated chromatin regions (Figure 1A). The MAN1-BioID2 transgenic plants were treated with 50 μM free biotin for proximity labeling. After free biotin depletion by desalting chromatography, the total biotinylated proteins were affinity-purified with streptavidin-coated beads before being subject to label-free quantitative MS with three biological replicates. Protein samples from biotin mock-treated plants expressing YFP-BioID2 (Mock) and biotin-treated nontransgenic plants (NT) were used as controls. The MS peptide intensity values from all samples were used for ratiometric protein enrichment analysis (Figure 1B, left panel). A total of 73 significantly enriched candidates were identified using cutoffs p value < 0.1 and foldchange > 2 compared with both controls (Table S1). Among significantly enriched MAN1 preys, we found lamin-like proteins CRWN1 and CRWN4 and at least six potential chromatin-associated proteins, including a histone modifier, transcription factors, and other DNA-binding proteins (Figure 1B, right panel), supporting that MAN1 is associated with chromatin at the INM in Arabidopsis.

In the identified MAN1 proxitome, a protein encoded by At1g28760 that contains six predicted transmembrane helices attracted our special attention, not only because it is ranked as the top transmembrane protein on the MAN1 prey list but also because its homolog (At5g67610) was recently identified by us as a plant nuclear envelope transmembrane protein (PNET2) using subtractive proteomics in Arabidopsis (Tang et al., 2020). We designated At1g28760 as PNET2\_A, At5g67610 as PNET2\_B and a third homologous gene At3g49840 found in the Arabidopsis genome as PNET2\_C (Figure 1C). Identification of PNET2\_A by proximity labeling using MAN1 as bait suggests that PNET2\_A is a potential INM protein.

#### PNET2s are conserved nuclear membrane proteins

Phylogenetic analysis revealed that PNET2 belongs to a protein family that broadly exists in both plants and animals (Figure 1D). Loss of PNET2 homolog (NEMP1) has been reported to lead to defects in neural development in Xenopus (Mamada et al., 2009; Shibano et al., 2015) and sterility or early loss of fertility in different animal species (Tsatskis et al., 2020). Alignment of plant PNET2 and animal NEMP1 proteins revealed an overall similar domain architecture but considerable sequence variations, particularly in the N terminus of the protein (Figure S1D). In the middle, all proteins contain a multiple-transmembrane domain but show a difference in the number of predicted transmembrane helices and thus protein topology (e.g., six TMs in PNET2 and five TMs in NEMP1). Although the C-terminal domain of the proteins is relatively conserved, NEMP1 contains a BAFbinding site near the C-terminal end, which has been shown to interact with the chromatin-binding protein BAF and is required for NEMP1 function in Xenopus (Mamada et al., 2009; Shibano





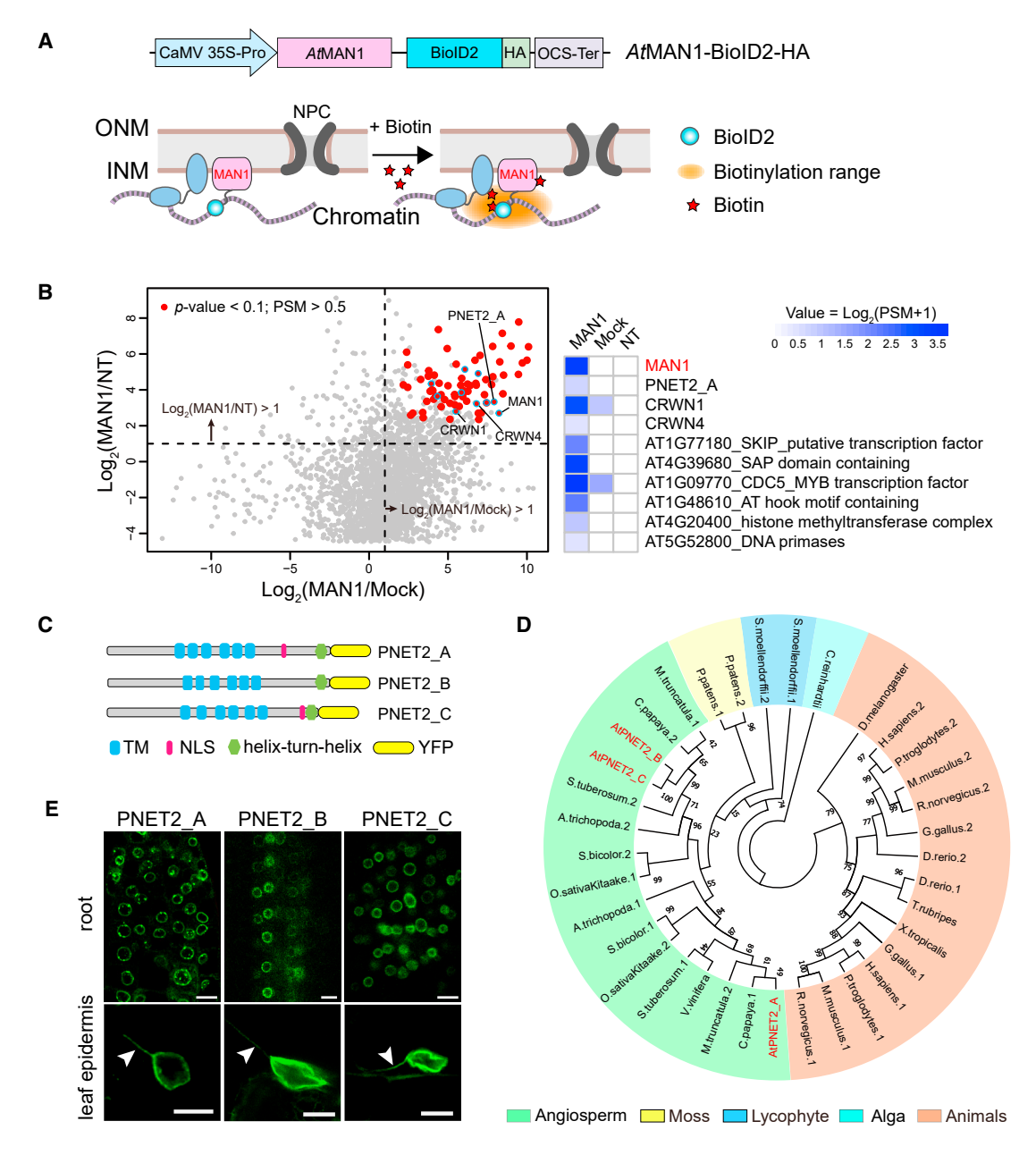


Figure 1. PNET2s are conserved inner nuclear membrane proteins

(A) Schematic diagrams of MAN1-BioID2-HA construct and identification of MAN1 proximal proteins that are potentially involved in chromatin tethering at the INM

(B) Scatter plot showing significantly enriched proteins identified by proximity labeling proteomics using MAN1-BioID2-HA as bait in Arabidopsis. Protein samples from nontransgenic WT plants with biotin treatment (NT) and transgenic YFP-BioID2-HA plants without biotin treatment (Mock) were used as controls for ratiometric analysis. Three biological replicates were used for each sample. Significantly enriched proteins were selected using p value < 0.1, fold-change > 2, and peptide spectrum match (PSM) > 0.5 as cutoffs and are represented by red dots. Nucleoskeleton proteins and potential chromatin-associated proteins are circled by blue, and their normalized PSM values are plotted on a heatmap shown on the right.

(C) Protein domain structures of three PNET2 paralogs in Arabidopsis. TM, transmembrane helix; NLS, nuclear localization signal.

(D) Phylogenetic analysis of PENT2 and its homologs in plant and animal species using amino acid sequences. The neighbor-joining tree was generated using the maximum-likelihood method with 1,000 bootstraps in MEGA-X.

(E) Fluorescent imaging of root and leaf epidermal cells using 35S:PNET2\_A/B/C-YFP transgenic Arabidopsis. Arrowheads indicate tail-like extension structures of the nuclear membrane. Bars: 10  $\mu m$ .

See also Figure S1 and Table S1.



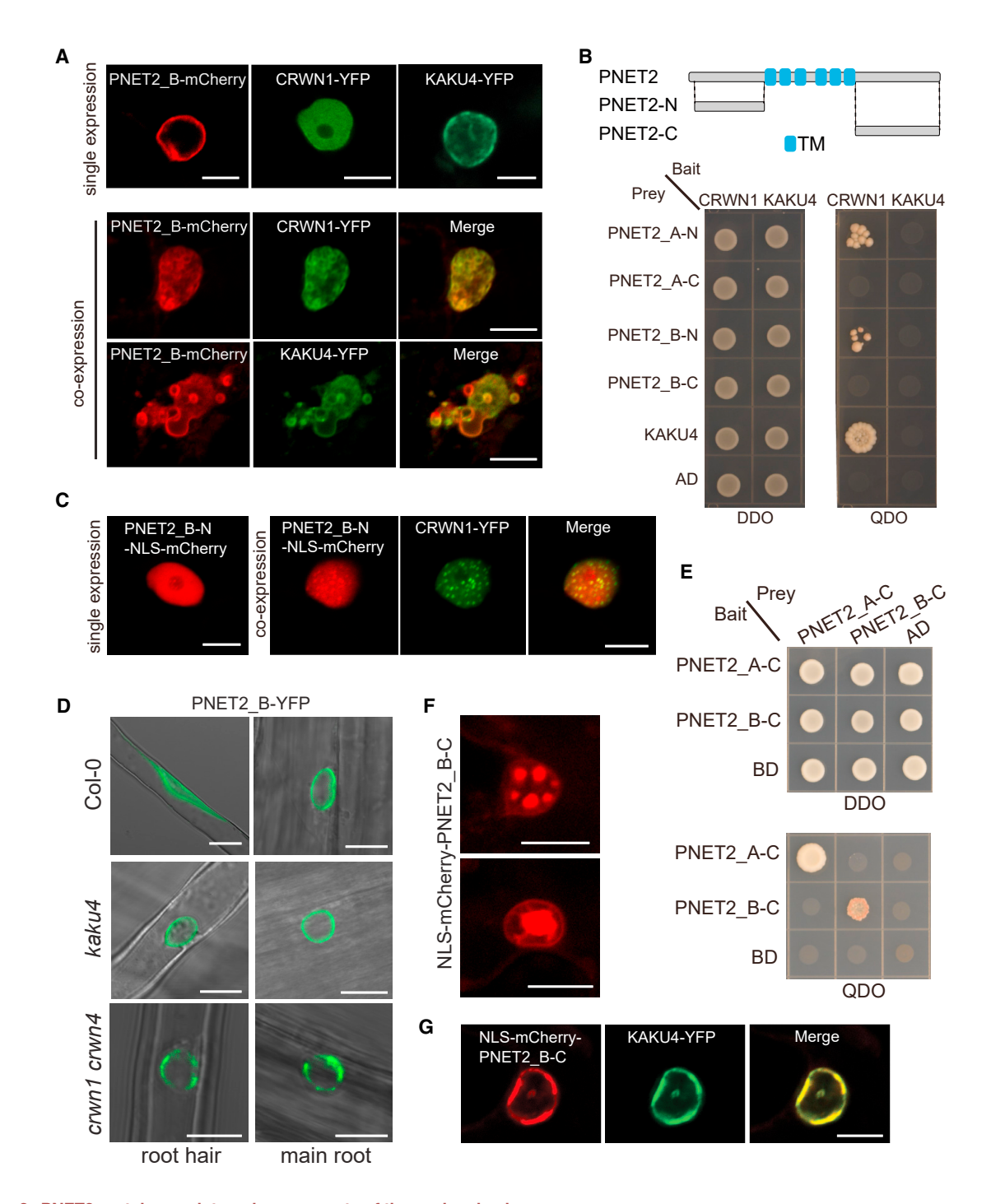


Figure 2. PNET2 proteins are integral components of the nuclear lamina

(A) Transient protein expression in N. benthamiana. PNET2\_B-mCherry, CRWN1-YFP, and KAKU4-YFP were individually expressed (upper panel). PNET2\_B-mCherry, CRWN1-YFP, and KAKU4-YFP were individually expressed (upper panel). mCherry was coexpressed with CRWN1-YFP or KAKU4-YFP (lower panel). Leaf epidermal cells were imaged, and nuclei are shown.

- (B) Yeast-two-hybrid (Y2H) analysis using PNET2 N- or C-terminal domains as the prey and nucleoskeletal protein CRWN1 and KAKU4 at the bait. Diploid yeasts after mating were grown on DDO (SD-Leu/-Trp) and QDO (SD-Leu/-Trp/-His/-Ade) media for 3 days before images were taken. Schematic of PNET2 constructs (N/C-terminal domains) used for Y2H assays is shown on the top.
- (C) Transient expression of the N-terminal domain of PNET\_B fused with an NLS signal and mCherry at the C-terminal end (PNET2\_B-N-NLS-mCherry). Subcellular localization of PNET2\_B-N-NLS-mCherry when individually expressed and coexpressed with CRWN1 is shown.
- (D) Fluorescence imaging of root hair and main root cells using 35S:PNET2\_B-YFP transgenic Arabidopsis seedlings in WT (Col-0) and the kaku4 and crwn1 crwn1 mutant background.

(legend continued on next page)

#### Article



et al., 2015). However, this motif is absent in PNET2 across the plant kingdom, which is consistent with the absence of BAF homologs in plants and suggests a function of PNET2 in a BAF-independent manner.

To confirm the NE localization of PNET2, we tagged YFP to the carboxyl terminus of PNET2 (PNET2-YFP), which we showed later is a functional fusion (see below). Using both transient expression in Nicotiana benthamiana and stable expression in Arabidopsis, we found that PNET2\_A/B/C-YFP proteins were all exclusively targeted to the nuclear membrane (Figures 1E, S1E, and S1F). Notably, in 35S:PNET2\_A/B/C-YFP transgenic plants, overexpression of PNET2 could result in nuclear membrane deformation in leaf epidermal cells, where nuclei were frequently observed to exhibit a tail-like extension structure (Figure 1E), reminiscent of the nuclear morphology observed when overexpressing the plant nucleoskeletal protein KAKU4 (Goto et al., 2014), suggesting a link between PNET2 and the nucleoskeleton.

#### **PNET2s** interact with the nucleoskeleton

Supporting the above idea, when we transiently coexpressed PNET2\_B with the Arabidopsis nucleoskeletal protein CRWN1 in N. benthamiana, they induced the formation of small circular membrane structures at the NE, which was not observed when PNET2\_B and CRWN1 were individually expressed (Figure 2A). Furthermore, coexpressing PNET2\_B with KAKU4 induced even more severe NE deformation and failure in maintaining the intact NE morphology in about 80% of cells with coexpression (Figure 2A, lower panel). This appears to be a synergistic effect between PNET2\_B and KAKU4, which was not observed when KAKU4 was expressed alone at a similar level in N. benthamiana (Figure 2A, upper panel) and mimics the effect of co-overexpression of KAKU4 and CRWN1 as reported before (Goto et al., 2014). Coexpression of PNET2\_A with KAKU4 also induced nuclear deformation but to a lesser extend compared with PNET2\_B (Figure S2A).

To determine whether PNET2s directly interact with the nucleoskeleton, we performed yeast two-hybrid (Y2H) assays between PNET2 proteins and CRWN1/KAKU4. We found that the N-, but not C-, terminal domain of PNET2\_A and PNET2\_B physically interacted with CRWN1 in yeast (Figure 2B), suggesting that PNET2 directly binds with the nucleoskeleton. In line with this observation, coexpression of CRWN1 with the soluble N-terminal domain of PNET2 led to re-localization of both proteins to the same punctate subnuclear structure (Figures 2C and S2B), further supporting a physical association. Although no interactions were detected between PNET2 and KAKU4 in yeast, a robust BiFC signal could be seen between the full-length PNET2\_A/B and KAKU4 at the nuclear surface during transient expression assay in plant cells that did not display serious NE deformation (Figure S2C). Together, these data indicate that PNET2 proteins are tightly associated with the plant nucleoskeleton, at least partly through directly interacting with CRWN1. Moreover, loss of CRWN1 and its functional homolog CRWN4 in Arabidopsis is sufficient to change the localization pattern of PNET2\_B. Compared with an even distribution at the NE in the WT background, PNET2\_B-YFP displayed a locally clustered pattern in crwn1 crwn4 double mutant plants (Figure 2D), although the protein still appeared to associate with the NE. These data suggest a primary role of CRWN proteins in determining the proper distribution of PNET2 beneath the INM but also implicates a possible nucleoskeleton-independent INM retention mechanism for PNET2. In contrast to CRWNs, loss of KAKU4 was not sufficient to cause a visible effect on the NE distribution of PNET2 B.

The C-terminal domain of PNET2\_A and PNET2\_B did not interact with CRWN1 or KAKU4 in yeast; however, it conferred homomeric interaction (Figure 2E). The PNET2 C terminus contains a predicted intrinsically disordered region (IDR) that may promote liquid-liquid phase separation (LLPS) (Figure S2D). Consistently, when we transiently expressed the PNET2\_A/B C-terminal domain fused with a nuclear localization signal (NLS-mCherry-PNET2\_A/B-C) in N. benthamiana, the protein did not distribute freely within the nucleus but formed dropletlike structures or large aggregates in the nucleoplasm (Figures 2F and S2B). Interestingly, when coexpressed with KAKU4-YFP, NLS-mCherry-PNET2\_A/B-C relocalized to the nuclear surface and completely overlapped with KAKU4-YFP (Figures 2G and S2B). Recruitment of the PNET2 C-terminal domain by KAKU4 to the NE suggests that an N-terminal-domain-independent mechanism also contributes to PNET2's association with the nucleoskeleton and further supports that PNET2 is part of the plant NL.

#### PNET2s are intimately associated with chromatin

To investigate the role of PNET2 in the plant NL, we generated transgenic lines expressing PNET2\_A-BioID2 and PNET2\_B-BioID2, respectively, and performed proximity labeling proteomics to profile PNET2\_A/B proxitome. Among probed candidates with high confidence (p value < 0.1 and fold-change > 2), we identified CRWN1, CRWN4, and KAKU4 (Figures 3A and 3B; Table S2), reinforcing our conclusion that PNET2s interact with the nucleoskeleton. Intriguingly, we also found that histone H2 proteins are significantly enriched in the proxitome probed by both PNET2\_A-BioID2 (p value = 7.8e-04) and PNET2\_B-BioID2 (p value = 9.0e-04), and histone H2 proteins are among top preys identified by PNET2\_B (Table S2), suggesting a close association of PNET2 with chromatin. Supporting this hypothesis, when we immunoprecipitated PNET2\_A-YFP that was transiently expressed in N. benthamiana, we could detect clear enrichment of native histone H2A proteins using an anti-histone H2A antibody (Figure 3C).

In comparison, we observed no enrichment of core histone proteins in MAN1 probed proxitome; instead, DNA-binding proteins including an SAP-domain-containing protein, an AT-hook motif-containing protein, and transcription factors were identified (Figure 1B; Table S1). These data indicate that the chromatin may establish contacts with MAN1 and PNET2 through distinct

<sup>(</sup>E) Y2H analysis using PNET2\_A/B C-terminal domains.

<sup>(</sup>F) Transient expression of PNET2\_B C-terminal domain fused with an NLS signal and mCherry at the N-terminal end (NLS-mCherry-PNET2\_B-C).

<sup>(</sup>G) Transient coexpression of NLS-mCherry-PNET2\_B-C with KAKU4-YFP. Nuclei are shown. Bars: 10 μm.



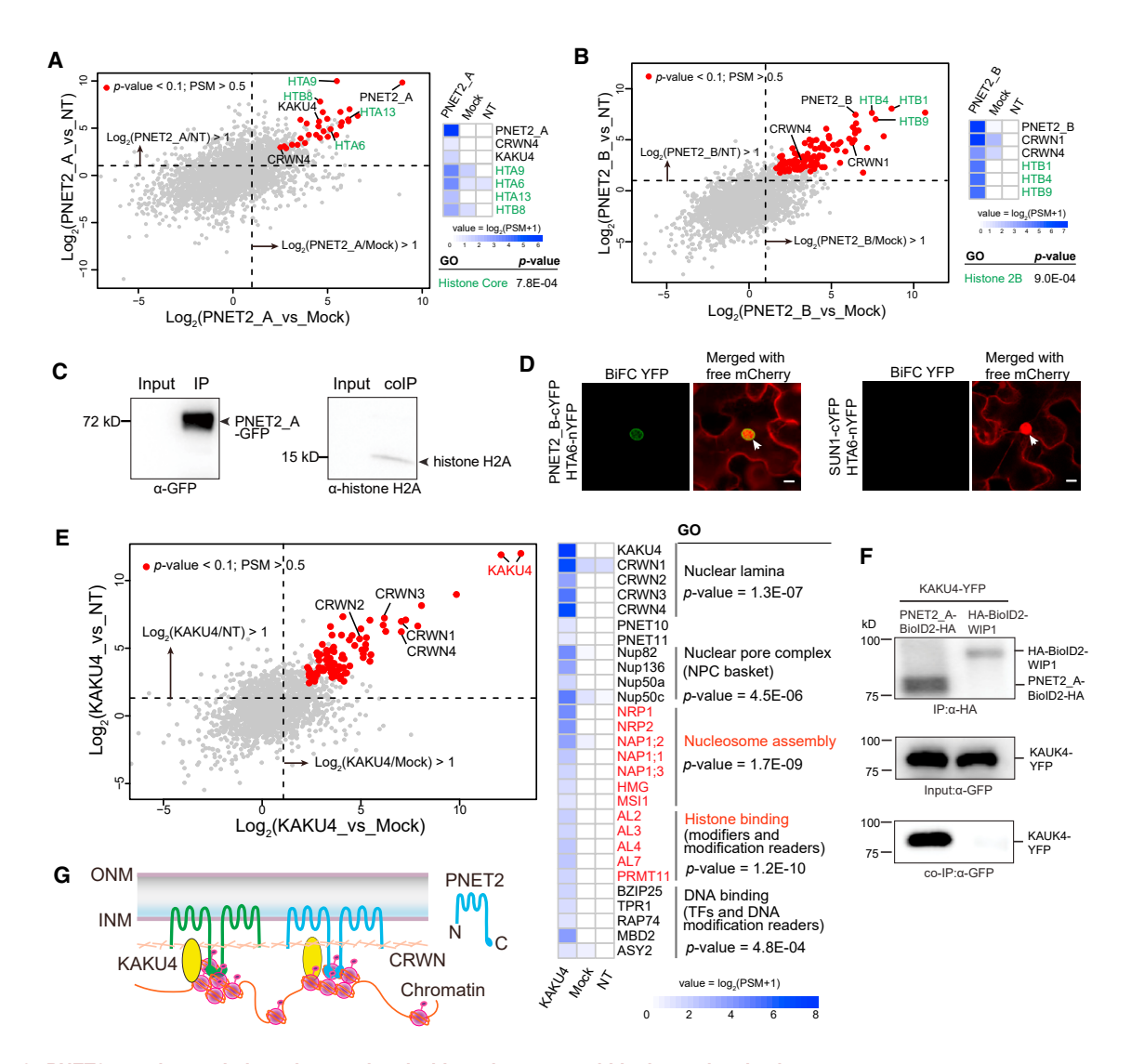


Figure 3. PNET2 proteins are intimately associated with nucleosomes within the nuclear lamina

(A and B) Scatter plots showing significantly enriched Arabidopsis proteins identified by proximity labeling proteomics using PNET2 A-BioID2-HA (A) and PNET2\_B-BioID2-HA (B) as bait. NT and mock samples were used as controls for ratiometric analysis, and three biological replicates were used for each sample. Significantly enriched protein candidates were selected using p value < 0.1, fold-change > 2, and PSM > 0.5 as cutoffs and are represented by red dots. Histone proteins are labeled in green, and their GO enrichment statistics are shown on the bottom right. The normalized PSM values of text-labeled protein preys are plotted on a heatmap shown on the right.

- (C) PNET2\_A-YFP was transiently expressed in N. benthamiana. The total protein was extracted and immunoprecipitated using GFP-trap beads. Subsequent immunoblotting was performed using anti-GFP and anti-histone H2A antibodies.
- (D) Bimolecular fluorescence complementation (BiFC) assay by transiently coexpressing histone H2A6-nYFP and PNET2\_B-cYFP or SUN1-cYFP in N. benthamiana. Free mCherry was coexpressed as a marker. Arrows indicate nucleus. Bars: 10 um.
- (E) Scatter plot showing significantly enriched Arabidopsis proteins identified by proximity labeling proteomics using KAKU4-BioID2-HA as bait. Significantly enriched protein candidates were selected using p value < 0.1, fold-change > 2, and PSM > 0.5 as cutoffs and are represented by red dots. Heatmap of normalized PSM values and GO analysis of significantly enriched preys are shown on the right.
- (F) Coimmunoprecipitation assay between PNET2\_A and KAKU4. Total protein was extracted from N. benthamiana leaves transiently coexpressing PNET2\_A-BioID2-HA and KAKU4-YFP and incubated with agarose beads conjugated with anti-HA antibody. IP samples were immunoblotted with anti-GFP and anti-HA antibodies. The outer nuclear membrane protein WIP1 was used as the control.
- (G) Schematic showing a model in which PNET2 protein is anchored at the INM through directly interacting with CRWN1 and intimately associates with nucleosome-enriched chromatin regions together with KAKU4. See also Figure S3 and Table S2.

protein interactions. Besides MAN1, another INM protein SUN1 also did not probe histone proteins using proximity labeling proteomics (Huang et al., 2020; Tang et al., 2020). Consistently, SUN1 did not interact with histone H2 proteins in BiFC assays (Figures 3D and S3A). In contrast, we detected clear complemented fluorescence between PNET2\_B with histone H2 proteins at the nuclear periphery using BiFC (Figures 3D and S3A), supporting an intimate association of PNET2 with chromatin at

**Article** 



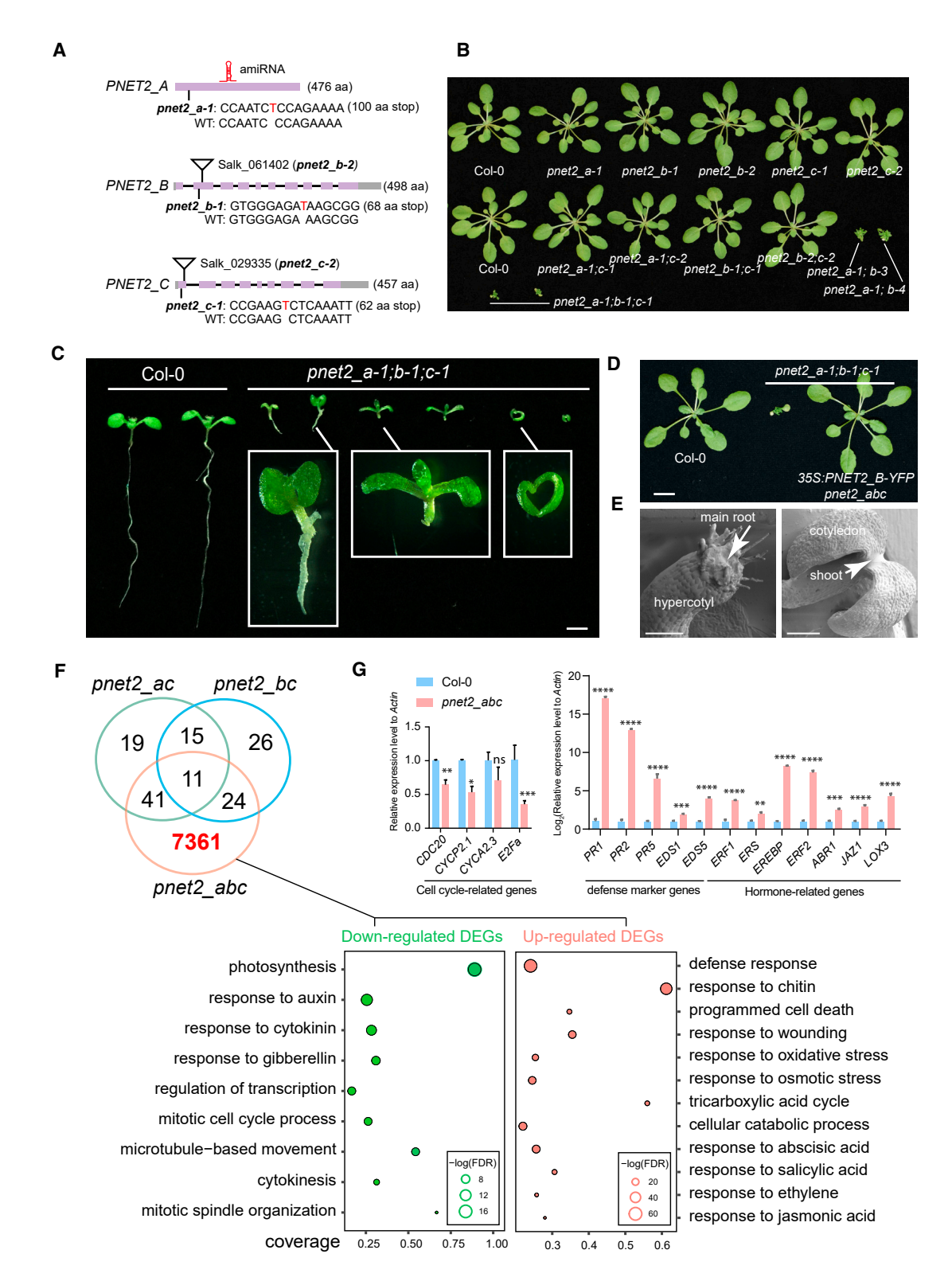


Figure 4. PNET2s are redundantly required for plant survival and loss of PNET2s leads to global transcriptional reprogramming

(A) The pnet2 T-DNA and CRISPR mutant alleles and the position of artificial miRNA. All Cas9-generated mutations result in premature stop codons at the location indicated .

(B) 4-week-old soil-grown plants. WT, pnet2\_a/b/c single mutants, pnet2\_ac/bc double mutants, two independent pnet2\_b CRISPR lines in the pnet2\_a-1 background, and pnet2\_abc triple mutants are shown. All CRISPR pnet2\_mutations were confirmed by sequencing.

(C) 4-day-old WT and pnet2\_abc triple mutant plants grown on half MS plates are shown. Bar: 1 cm.



Article

the INM. However, we did not detect physical interactions between PNET2\_A/B with histone H2 using Y2H assays (Figure S3B), suggesting that the association may require intermediate factors or that PNET2 may interact with histone H2 proteins that bear specific epigenetic modifications.

## PNET2 and KAKU4 are associated with nucleosomes in the NL

Enrichment of core histone proteins in the PNET2 proxitome indicates that PNET2s associate with nucleosomeenriched chromatin regions, potentially within the NL. To strengthen this hypothesis, we tested if PNET2-interacting nucleoskeletal proteins also associate with nucleosome-enriched chromatin. We performed proximity labeling proteomics using transgenic Arabidopsis plants expressing CRWN1-BioID2 and KAKU4-BioID2, respectively. To our surprise, we did not detect histone proteins or DNA-binding proteins among high-confident CRWN1 preys (p value < 0.1 and fold-change > 2), even when we used less stringent cutoffs (p value < 0.3). However, other known CRWN1 proximal proteins such as SUN1/2, CRWN4, and KAKU4 were identified (Table S2). In contrast, in the KAKU4 proxitome that is composed by 85 high-confident preys (Table S2), we identified a significant enrichment of the nucleosome assembly protein (NAP) family (seven members, p value = 1.7e-09), including NRP1 and NRP2 that directly bind histone H2 proteins (Figure 3E). In addition, other histone-binding proteins including histone modifiers and modification readers were also highly enriched (p value = 1.2e-10). KAKU4 also probed all four CRWN proteins and NPC basket components, validating its functional targeting to the NL. This result strongly supports an intimate association of KAKU4 with the nucleosome core in the NL.

Because both PNET2 and KAKU4 are closely associated with nucleosome core histone H2 proteins and PNET2 C-terminal domain can be engaged by KAKU4 to the nuclear periphery, we propose that the two proteins are closely associated despite that no direct protein interaction was detected by Y2H. Supporting this hypothesis, KAKU4 can be co-immunoprecipitated by PNET2\_A *in planta* (Figure 3F). Together, these data prompted us to propose a model in which PNET2 protein physically binds CRWN1 for its proper distribution beneath the INM, where it forms a matrix with KAKU4 by co-associating with nucleosome-enriched chromatin in the NL (Figure 3G).

#### PNET2s are essential for plant survival

To assess the functional importance of PNET2 in plants, we generated *pnet2* mutants in *Arabidopsis*. We designed guide RNAs that individually target the three *PNET2* genes and

obtained CRISPR pnet2 single mutants, including pnet2\_a-1, pnet2\_b-1, and pnet2\_c-1. In all three mutant lines, Cas9-generated mutations led to frameshifts and premature stop codons near the beginning of PNET2 genes, likely resulting in loss of function (Figure 4A). In addition, we obtained available T-DNA insertion mutant lines for PNET2\_B (Salk\_061402, pnet2\_b-2) and PNET2\_C (Salk\_029335, pnet2\_c-2), in which the expression of corresponding PNET2 genes was reduced by 90% or more (Figure S4A). We found that none of the pnet2 single mutants showed obvious defects in growth and development compared with WT (Figure 4B). Next, we generated a series of pnet2 double mutants through genetic crosses, including pnet2\_a-1 pnet2\_c-1, pnet2\_a-1 pnet2\_c-2, pnet2\_b-1 pnet2\_c-1, and pnet2\_b-2 pnet2\_c-2. We found that all pnet2\_ac and pnet2\_bc double mutants display no discernible phenotypes (Figure 4B). However, when we used CRISPR to knockout PNET2\_B in the pnet2\_a-1 background, we were able to identify multiple independent pnet2\_ab double mutant alleles that showed a striking phenotype with severely disrupted growth and development (Figure 4B). Moreover, we re-generated the pnet2\_a-1 mutation in the pnet2\_b-1 pnet2\_c-1 background using CRISPR. The resulting pnet2\_a-1 pnet2\_b-1 pnet2\_c-1 triple mutant shows a further enhanced growth defect compared with pnet2\_ab lines (Figures 4B and 4C). To further validate this phenotype, we knocked down PNET2 A in the pnet2 b-2 pnet2\_c-2 double mutant background using an artificial micro-RNA, which led to a series of hypomorphic triple mutant phenotypes in independent T1 transgenic lines, and in the most severe lines, seedlings could barely grow (Figure S4B), similar to pnet2 a-1 pnet2 b-1 pnet2 c-1 plants. Ectopic expression of PNET2\_B-YFP rescued the pnet2\_a-1 pnet2\_b-1 pnet2\_c-1 triple mutant phenotype (Figure 4D), confirming that the observed phenotype is caused by loss of PNET2 and suggesting that PNET2s are redundantly required for plant development and survival.

The triple mutant is maintained in the <code>pnet2\_a-1</code> (heterozygous) <code>pnet2\_b-1</code> <code>pnet2\_c-1</code> (homozygous) background. Detailed dissection of the segregating offspring revealed that the triple mutant seedlings lack the apical shoot (72.4%, 123/170), the main root (15.8%, 27/170), or both (11.8%, 20/170) (Figures 4C and 4E), which resulted in extremely restricted growth and eventually seedling lethality. Based on the phylogenetic analysis (Figure 1D) and the above genetic data, we postulate that PNET2\_C may be a functional duplication of PNET2\_B, but the native expression level is not sufficient to complement the loss of PNET2\_B. Indeed, PNET2\_B expresses at a much higher level than PNET2\_C in almost all tissues in <code>Arabidopsis</code> (Figure S4C). For a complete <code>pnet2</code> knockout background, we used the

<sup>(</sup>D) Complementation of the *pnet2\_abc* triple mutant growth phenotype by ectopically expressing *PNET2\_B-YFP* (T2 generation). 4-week-old soil-grown plants are shown. Bar: 1 cm.

<sup>(</sup>E) Scanning electron microscopy images of 4-day-old pnet2\_abc triple mutant seedlings, which lack the main root and shoot apex. Bars: 400 µm.

<sup>(</sup>F) Venn diagram showing overlaps of differentially expressed genes (DEGs) in pnet2\_ac, pnet2\_bc, and pnet2\_abc mutant plants compared with WT using data from RNA-seq analysis. Three biological replicates were used for each RNA-seq sample, and DEGs were selected using cutoffs p value < 0.01 and fold-change > 2 or < 0.5. GO enrichment analysis of DEGs in the pnet2\_abc mutant is shown in the lower panel. Representative GO terms are presented.

<sup>(</sup>G) The relative expression level of cell-cycle-related genes, defense marker genes, and stress-related hormone responsive genes in 3-day-old seedlings was measured using real-time qPCR. The gene expression level was normalized to that in WT. *Actin* was used as the reference gene. Data are represented as means  $\pm$  SDM (n = 2 biological replicates), and Student's t tests were performed using WT as control. Similar results have been obtained twice. \*p < 0.05, \*\*p < 0.01, \*\*\*p < 0.001, \*\*\*\*p < 0.0001. ns stands for not significant.

**Article** 



pnet2\_abc triple mutant rather than the pnet2\_ab double mutant for functional analysis in the remaining studies.

#### Loss of PNET2 leads to global transcriptional reprogramming

To better understand the observed defects caused by loss of PNET2s, we performed whole-genome RNA-seq profiling using 1-week-old seedlings (GEO: GSE147968). We found no significant transcriptome change in pnet2\_ac and pnet2\_bc double mutants (Figure S4D), and both double mutants induced less than 100 differentially expressed genes (DEGs) compared with WT (Figure 4F). However, a dramatic transcriptome reprogramming was observed in the pnet2\_abc triple mutant with 7,457 significant DEGs identified (p value < 0.01 and fold-change > 2 compared with WT) (Figures 4F and S4E; Table S3). Gene Ontology analysis revealed that the 3,836 significantly downregulated DEGs in pent2\_abc are highly enriched in cell-cyclerelated processes and responses to phytohormones that promote cell division (e.g., auxin and cytokinin), consistent with the arrested seedling growth and development (Figure 4F). On the other hand, innate immune responses and signaling pathways of various abiotic and biotic stress-responsive phytohormones, including salicylic acid (SA), jasmonic acid (JA), abscisic acid (ABA), and ethylene (ET), are simultaneously activated in the pnet2 abc triple mutant, reminiscent of the transcriptional misregulation induced upon loss of CRWNs in Arabidopsis (Choi and Richards, 2020; Choi et al., 2019), albeit to a more severe extent in the pnet2 mutant. To confirm this result and avoid secondary transcription responses as much as possible, we performed quantitative real-time PCR using 3-day-old seedlings. Again, we detected significantly repressed cell division activity and activated defense- and stress-related hormone marker gene expression in the pnet2\_abc mutant (Figure 4G). Although we are aware that using young seedlings still cannot completely exclude possible secondary effects in transcription responses, these results support that PNET2 is essential for maintaining the growth-versus-stress gene expression homeostasis during early seedling development. We hypothesize that the inversed growth-versus-stress transcriptional landscape is at least partially induced by compromised NL and NL-chromatin association due to the loss of PNET2 proteins. This may lead to disruptions in the spatial organization of chromatin, nucleosome arrangement, and epigenetic states, which could contribute to alterations in chromatin activities and de-repression of stressrelated genes.

#### **PNET2** is required for maintenance of proper chromatin organization

To explore possible changes in chromatin architectures upon loss of PNET2, we performed HiC analysis and compared the chromatin interaction patterns in 10-day-old WT and pnet2\_abc triple mutant seedlings. Interestingly, at the global level, we found that cis interactions are locally enhanced for intra-chromosomal regions in the triple mutant (Figure 5A, diagonal region). Consistently, more locally formed chromatin loops (spanning  $\sim$ 1,000 base pairs) that mediate gene-gene interactions were identified in the pnet2\_abc mutant compared with WT (Figure S5A). In addition, it appears that the interactions between heterochromatic chromocenters on different chromosomes, as well as chromocenters of each chromosome with euchromatins of all chromosomes, are also enhanced in the pnet2\_abc mutant. However, distant intra-chromosomal interactions as well as inter-chromosomal interactions are mostly attenuated upon loss of PNET2 (Figure 5A, off-diagonal region), suggesting a generally compromised higher-order chromatin packing in those regions. This pattern is also supported by faster interaction decay within 5 million base pairs from the focal point in the pnet2\_abc triple mutant than in WT (Figure S5B). Consistent with the globally reduced chromatin packing revealed by HiC, we also found that the pnet2\_abc triple mutant exhibits a peculiar chromatin staining by 4',6-diamidino-2-phenylindole (DAPI). Although the formation of chromocenters and the overall DNA content did not appear to be affected in the mutant (Figures 5B and S5C), the DAPI staining of nuclei is largely diminished in pnet2\_abc cells from various tissues (Figure 5B), supporting a disintegrated chromatin organization. Moreover, we characterized the interaction between heterochromatic regions located in euchromatins termed as interactive heterochromatic islands (IHIs) or KNOT ENGAGED ELEMENTs (KEEs), which are featured by forming interaction hubs within network connection (Grob et al., 2014). There are totally eleven KEEs identified in WT (KEE 1  $\sim$  KEE 11). Interestingly, KEE 11 is missing in the pnet2\_abc mutant while two novel KEEs (KEE 12 and KEE 13) were identified (Figure S5D), suggesting a complicated change in chromatin architecture as a result of loss of PNET2. We also characterized and compared the profiles of A/B (euchromatic/heterochromatic) compartments or loose/compacted structural domains (LSD/ CSDs) in WT and pnet\_abc plants. We found that although most A/B compartments are stable, many compartment-switching events (A-to-B or B-to-A) could be captured in the pnet2\_abc mutant, and those events were not evenly distributed on different chromosomes (Figures 5C, 5D, and S5E). Together, these analyses suggest significant alterations in chromatin packing and potential changes in chromatin activities in the absence of PNET2. They also support the hypothesis that PNET2s play a role in engaging chromatin in the NL and are required for maintaining proper genome organization.

#### **DISCUSSION**

We identified PNET2s as plant INM proteins and showed that they are integral components of the plant NL by tightly associating with both the nucleoskeleton and chromatin. Interaction of PNET2 with the nucleoskeleton may involve a combined molecular and biophysical mechanism. While the PNET2 N terminus makes direct contact with CRWN1 through protein-protein interaction, its C terminus mediates homomeric association, which could further promote multivalent interactions within the PNET2-nucleoskeleton network. Furthermore, because the PNET2 C terminus contains predicted IDRs with high confidence and overexpression of this domain leads to the formation of large condensates in vivo, it is possible that PNET2 C terminus may undergo LLPS. Interestingly, CRWN proteins also belong to plant IDR-containing proteins that may undergo LLPS (Huang et al., 2021). Physical interaction between PNET2 and CRWN1 and potential LLPS of both proteins may together contribute to establishing a separated phase/environment for the plant NL



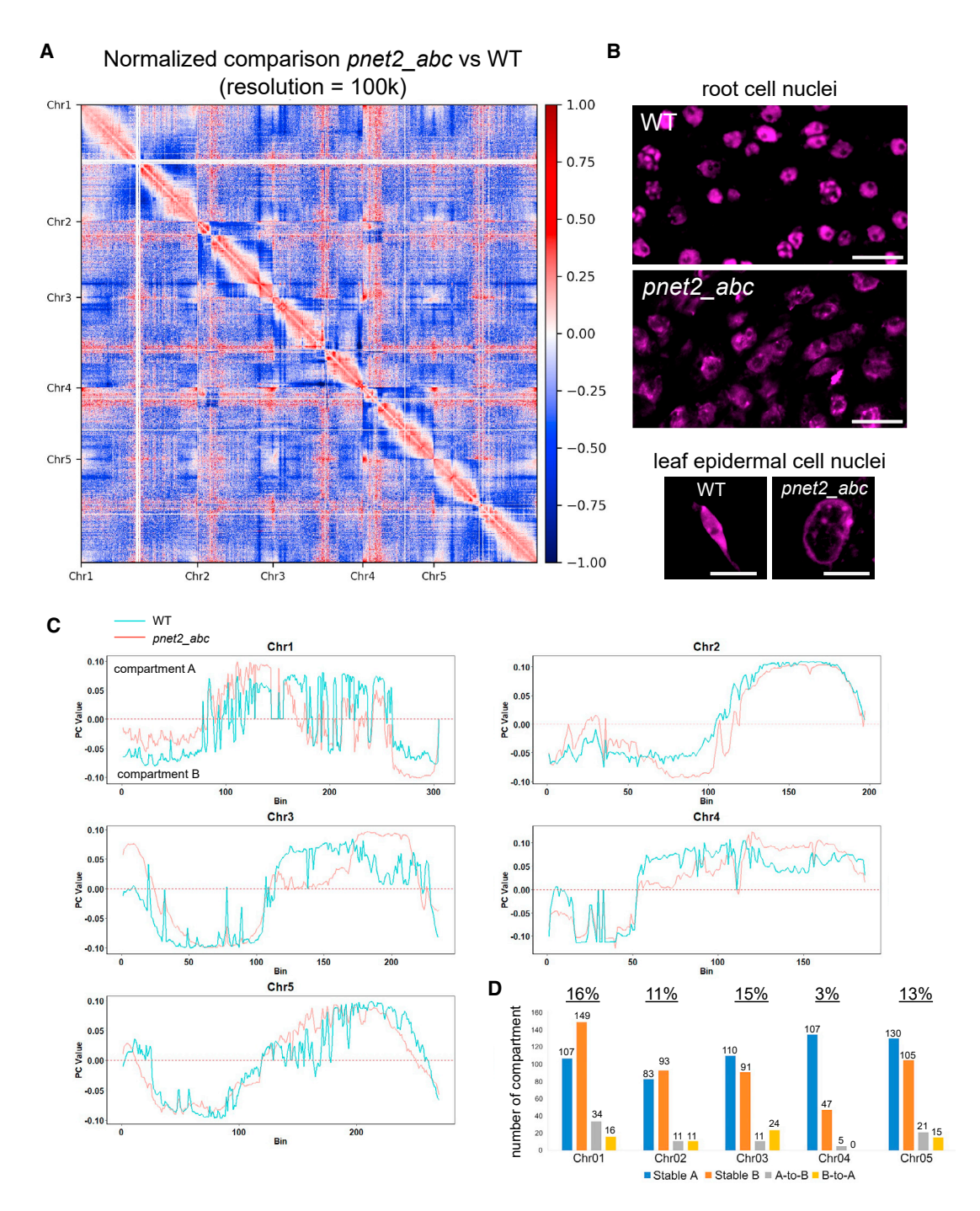


Figure 5. Loss of PNET2s induces global changes in chromatin packing and compartmental switching

(A) Differential chromatin interaction 2D plot showing changes in chromatin interactions (pnet2\_abc versus WT) captured by HiC at 100-kb resolution. Lower interaction frequency in pnet2\_abc relative to WT is depicted in darker blue and vice versa in darker red.

<sup>(</sup>B) DAPI staining of root and leaf epidermal cells in 7-day-old Arabidopsis seedlings.

<sup>(</sup>C) Compartment principal component (PC) values of each 100-kb bin along each chromosome in WT and pnet2\_abc plants. Positive and negative PC values denote A/B (euchromatic/heterochromatic) compartment status, respectively.

<sup>(</sup>D) Compartment category summary in the pnet2\_abc mutant compared with WT. A-to-B and B-to-A represent compartment-switching events. The percentage of switched compartments within each chromosome detected in the pnet2\_abc mutant compared with WT is labeled at the top. See also Figure S5.

Article



meshwork as well as the NL-chromatin matrix underneath the NE.

Proximity labeling proteomics revealed that both PNET2 and KAKU4 are closely associated with nucleosome-enriched chromatin at the nuclear periphery, suggesting that they may play a role in NL-mediated chromatin tethering. With the current data, we think that the PNET2 C terminus may be involved in building connections with chromatin for the following two reasons. First, although PNET2 lacks BAF-binding sites compared with its animal homolog NEMP1, both PNET2 and NEMP1 contain a conserved predicted bi-helical motif near the C-terminal end (Figure S1D), which bears structural similarity with the LAP2 LEM-like domain and SAP domain that can bind DNA. However, whether this motif mediates direct interactions with DNA in vivo awaits further investigation. Second, we found that PNET2 C terminus alone can be recruited to the nuclear surface by KAKU4, and this recruitment is independent of obvious NE targeting mechanisms and a physical interaction with KAKU4 detectable by Y2H. We speculate that the observed recruitment relies on its intimate association with nucleosomes at the NE, where KAKU4, PNET2, and nucleosome-enriched heterochromatin form a matrix to establish chromatin docking loci in the NL and contribute to the chromatin packing and higher-order organization. Tethering of chromatin to the NE supports nuclear mechanics (Schreiner et al., 2015), and indeed, loss of NEMP1 was recently shown to play a critical role in supporting metazoan NE mechanical stiffness (Tsatskis et al., 2020), suggesting that chromatin tethering may be a conserved function of PNET2

The role of plant NL in regulating chromatin organization and transcription activity is emerging. The nucleoskeletal protein CRWNs were found essential for the nonrandom chromatin organization at the NE (Hu et al., 2019) and required to suppress both abiotic and biotic stress-related gene expression (Choi and Richards, 2020; Choi et al., 2019; Guo et al., 2017; Sakamoto et al., 2020). CRWNs were recently reported to physically associate with a component of the histone modification complex polycomb repressive complex 2 (PRC2), which mediates repressive H3K27me3 histone modification (Mikulski et al., 2019). Loss of CRWNs results in decreased H3K27me3 of defense-related genes and altered chromatin distribution that correlates with suppression of copper-associated gene expression (Choi and Richards, 2020; Choi et al., 2019; Sakamoto et al., 2020). Interestingly, CRWN1 was also found subject to proteosome-dependent degradation upon infection by a bacterial pathogen and SA treatment (Guo et al., 2017), suggesting the plant NL may undergo dynamic changes in response to stress conditions, which potentially contributes to chromatin reorganization and transcription reprogramming. Adding more insight to this picture, we showed that loss of the INM component of the NL, PNET2, led to changes in chromatin architecture and dramatic transcription reprogramming that is featured by repression of cell division and activation of a broad spectrum of stress responses. This results in a pleiotropic and ultimately lethal phenotype in the pnet2 triple mutant. It is possible that PNET2 is important for proper chromatin packing and tethering to the NL, disruption of which leads to global changes in positioning-dependent gene activities. Indeed, compromised chromatin packing and euchromatic/heterochromatic compartment switches were observed in the pnet2\_abc mutant. Future research is needed to understand global epigenetic changes that are associated with the altered chromatin organization, and how that may lead to transcriptome reprogramming. Another possibility is that the regulation of chromatin packing and transcription programing by PNET2 is independent of each other. Under this second scenario, active retention of stress-related transcription factors to the nuclear periphery by PNET2 may be responsible for PNET2-dependent transcription regulation.

#### Limitations of the study

(1) We showed that PNET2 is closely associated with chromatin; however, little is known about the chromatin regions that are recruited by PNET2 to the nuclear periphery. It will be important to determine PNET2-assocaited genome sequences using ChIPseq analysis in the future. In addition, the molecular mechanism that mediates PNET2 interaction with chromatin is unclear. Future work will examine whether PNET2 can directly bind with DNA or DNA associated proteins. (2) Although dramatic transcriptome changes and potential euchromatic/heterochromatic compartment switches were observed in the pnet2\_abc mutant compared with WT, we were not able to find obvious correlation between DEGs identified by RNA-seg and genes in the compartment-switched chromatin regions defined by HiC. We think this is likely due to (a) the large number of DEGs, a significant portion of which do not directly response to loss of PNET2 but are involved in secondary or feedback transcriptional responses, (b) different mechanisms that regulate differential expression of a gene (i.e., compartment switching may trigger differential expression of only a portion but not all genes in the affected chromatin region), and (c) sampling using the whole seedling, which may mask the tissue or cell-type-specific correlation between the RNA-seq and HiC datasets. (3) The complete disruption of transcriptional balance between growth response and stress response in the absence of PNET2 is remarkable but still poorly understood. Future research will determine the molecular mechanism and key players (e.g., potential transcription factors) that work together with PNET2 to regulate in this process.

#### **STAR**\*METHODS

Detailed methods are provided in the online version of this paper and include the following:

- KEY RESOURCES TABLE
- RESOURCE AVAILABILITY
  - Lead contact
  - Material availability
  - Data and code availability
- EXPERIMENTAL MODEL AND SUBJECT DETAILS
  - Plant materials
- METHOD DETAILS
  - Plasmid construction
  - Phylogenetic analysis
  - O Bioinformatic analysis of PNET2s
  - O Transient protein expression and fluorescence imaging
  - O Proximity-labeling proteomics and ratiometric analysis
  - O RNA-seq and data analysis
  - RT-qPCR



- Yeast two-hybrid assay
- Co-immunoprecipitation
- O Flow cytometry of cell ploidy level
- O HiC and data analysis

#### SUPPLEMENTAL INFORMATION

Supplemental information can be found online at https://doi.org/10.1016/j. devcel.2021.11.002.

#### **ACKNOWLEDGMENTS**

The authors thank Dr. Eric Richards for sharing the crwn1 crwn4 double mutant. We also thank the technical director Bridget McLaughlin from UC Davis Campus Shared Flow Cytometry Resource for help with FACS analysis. This work was supported by the Changbai Mountain Scholar Program (to L.G.) and the USDA National Institute of Food and Agriculture (HATCH project CA-B-PLB-0243-H), National Science Foundation (NSF-MCB 2049931), Hellman Fellows fund, and startup funds from the Innovative Genomics Institute and the University of California Berkeley (to Y.G.).

#### **AUTHOR CONTRIBUTIONS**

Y.T. and Y.G. conceived the project. Q.D., T.W., and L.G. performed the HiC experiment and related data analysis. Y.T. conducted all the rest experiments and data analyses. Y.T., L.G., and Y.G wrote the paper.

#### **DECLARATION OF INTERESTS**

The authors declare no competing interests.

Received: July 8, 2021 Revised: September 24, 2021 Accepted: October 29, 2021 Published: November 24, 2021

#### **REFERENCES**

Amendola, M., and van Steensel, B. (2014). Mechanisms and dynamics of nuclear lamina-genome interactions. Curr. Opin. Cell Biol. 28, 61-68.

Aravind, L., Mazumder, R., Vasudevan, S., and Koonin, E.V. (2002). Trends in protein evolution inferred from sequence and structure analysis. Curr. Opin. Struct. Biol. 12, 392-399.

Ay, F., Bailey, T.L., and Noble, W.S. (2014). Statistical confidence estimation for Hi-C data reveals regulatory chromatin contacts. Genome Res 24,

Bi, X., Cheng, Y.-J., Hu, B., Ma, X., Wu, R., Wang, J.-W., and Liu, C. (2017). Nonrandom domain organization of the Arabidopsis genome at the nuclear periphery. Genome Res 27, 1162–1173.

Bione, S., Maestrini, E., Rivella, S., Mancini, M., Regis, S., Romeo, G., and Toniolo, D. (1994). Identification of a novel X-linked gene responsible for Emery-Dreifuss muscular dystrophy. Nat. Genet. 8, 323–327.

Brachner, A., and Foisner, R. (2011). Evolvement of LEM proteins as chromatin tethers at the nuclear periphery. Biochem. Soc. Trans. 39, 1735-1741.

Brachner, A., and Foisner, R. (2014). Lamina-associated polypeptide (LAP) 2alpha and other LEM proteins in cancer biology. Adv. Exp. Med. Biol. 773, 143-163.

Caputo, S., Couprie, J., Duband-Goulet, I., Kondé, E., Lin, F., Braud, S., Gondry, M., Gilquin, B., Worman, H.J., and Zinn-Justin, S. (2006). The carboxyl-terminal nucleoplasmic region of MAN1 exhibits a DNA binding winged helix domain. J. Biol. Chem. 281, 18208-18215.

Choi, J., and Richards, E.J. (2020). The role of CRWN nuclear proteins in chromatin-based regulation of stress response genes. Plant Signal. Behav. 15,

Choi, J., Strickler, S.R., and Richards, E.J. (2019). Loss of CRWN nuclear proteins induces cell death and salicylic acid defense signaling. Plant Physiol 179,

Cohen, T.V., Kosti, O., and Stewart, C.L. (2007). The nuclear envelope protein MAN1 regulates TGFbeta signaling and vasculogenesis in the embryonic yolk sac. Development 134, 1385-1395.

de Souza Junior, J.D., de Sa, M.F.G., Engler, G., and Engler, J.de A. (2016). Imaging nuclear morphology and organization in cleared plant tissues treated with cell cycle inhibitors. Methods Mol. Biol. 1370, 59-68.

Demmerle, J., Koch, A.J., and Holaska, J.M. (2012). The nuclear envelope protein emerin binds directly to histone deacetylase 3 (HDAC3) and activates HDAC3 activity. J. Biol. Chem. 287, 22080-22088.

Dong, Q., Li, N., Li, X., Yuan, Z., Xie, D., Wang, X., Li, J., Yu, Y., Wang, J., Ding, B., et al. (2018). Genome-wide Hi-C analysis reveals extensive hierarchical chromatin interactions in rice. Plant J 94, 1141-1156.

Du, Z., Zhou, X., Ling, Y., Zheng, Z., and Su, Z. (2010). agriGO: a GO analysis toolkit for the agricultural community. Nucleic Acids Res. 38, W64-W70.

Feng, S., Cokus, S.J., Schubert, V., Zhai, J., Pellegrini, M., and Jacobsen, S.E. (2014). Genome-wide Hi-C analyses in wild-type and mutants reveal high-resolution chromatin interactions in Arabidopsis. Mol. Cell 55, 694-707.

Finlan, L.E., Sproul, D., Thomson, I., Boyle, S., Kerr, E., Perry, P., Ylstra, B., Chubb, J.R., and Bickmore, W.A. (2008). Recruitment to the nuclear periphery can alter expression of genes in human cells. PLoS Genet 4, e1000039.

Goto, C., Tamura, K., Fukao, Y., Shimada, T., and Hara-Nishimura, I. (2014). The novel nuclear envelope protein KAKU4 modulates nuclear morphology in Arabidopsis. Plant Cell 26, 2143-2155.

Grob, S., Schmid, M.W., and Grossniklaus, U. (2014). Hi-C analysis in Arabidopsis identifies the KNOT, a structure with similarities to the flamenco locus of Drosophila. Mol. Cell 55, 678-693.

Grob, S., Schmid, M.W., Luedtke, N.W., Wicker, T., and Grossniklaus, U. (2013). Characterization of chromosomal architecture in Arabidopsis by chromosome conformation capture. Genome Biol 14, R129.

Grund, S.E., Fischer, T., Cabal, G.G., Antúnez, O., Pérez-Ortín, J.E., and Hurt, E. (2008). The inner nuclear membrane protein Src1 associates with subtelomeric genes and alters their regulated gene expression. J. Cell Biol. 182, 897-910.

Gu, Y., and Innes, R.W. (2011). The KEEP ON GOING protein of Arabidopsis recruits the ENHANCED DISEASE RESISTANCE1 protein to trans-Golgi network/early endosome vesicles. Plant Physiol 155, 1827-1838.

Gu, Y., Zebell, S.G., Liang, Z., Wang, S., Kang, B.-H., and Dong, X. (2016). Nuclear pore permeabilization is a convergent signaling event in effector-triggered immunity. Cell 166, 1526-1538.e11.

Guelen, L., Pagie, L., Brasset, E., Meuleman, W., Faza, M.B., Talhout, W., Eussen, B.H., de Klein, A., Wessels, L., de Laat, W., and van Steensel, B. (2008). Domain organization of human chromosomes revealed by mapping of nuclear lamina interactions. Nature 453, 948-951.

Guo, T., Mao, X., Zhang, H., Zhang, Y., Fu, M., Sun, Z., Kuai, P., Lou, Y., and Fang, Y. (2017). Lamin-like proteins negatively regulate plant immunity through NAC WITH TRANSMEMBRANE MOTIF1-LIKE9 and NONEXPRESSOR OF PR GENES1 in Arabidopsis thaliana. Mol. Plant 10, 1334-1348.

Hu, B., Wang, N., Bi, X., Karaaslan, E.S., Weber, A.-L., Zhu, W., Berendzen, K.W., and Liu, C. (2019). Plant lamin-like proteins mediate chromatin tethering at the nuclear periphery. Genome Biol 20, 87.

Huang, A., Tang, Y., Shi, X., Jia, M., Zhu, J., Yan, X., Chen, H., and Gu, Y. (2020). Proximity labeling proteomics reveals critical regulators for inner nuclear membrane protein degradation in plants. Nat. Commun. 11, 3284.

Huang, S., Zhu, S., Kumar, P., and MacMicking, J.D. (2021). A phase-separated nuclear GBPL circuit controls immunity in plants. Nature 594, 424-429.

Ikegami, K., Egelhofer, T.A., Strome, S., and Lieb, J.D. (2010). Caenorhabditis elegans chromosome arms are anchored to the nuclear membrane via discontinuous association with LEM-2. Genome Biol 11, R120.

Ishimura, A., Ng, J.K., Taira, M., Young, S.G., and Osada, S.-I. (2006). Man1, an inner nuclear membrane protein, regulates vascular remodeling by

#### **Article**



modulating transforming growth factor beta signaling. Development 133, 3919-3928

Jamin, A., and Wiebe, M.S. (2015). Barrier to Autointegration Factor (BANF1): interwoven roles in nuclear structure, genome integrity, innate immunity, stress responses and progeria. Curr. Opin. Cell Biol. 34, 61-68.

Jia, M., Shen, X., Tang, Y., Shi, X., and Gu, Y. (2021). A karyopherin constrains nuclear activity of the NLR protein SNC1 and is essential to prevent autoimmunity in Arabidopsis. Mol. Plant 14, 1733-1744.

Kim, D.I., Jensen, S.C., Noble, K.A., Kc, B., Roux, K.H., Motamedchaboki, K., and Roux, K.J. (2016). An improved smaller biotin ligase for BioID proximity labeling. Mol. Biol. Cell 27, 1188-1196.

Kim, D., Paggi, J.M., Park, C., Bennett, C., and Salzberg, S.L. (2019). Graphbased genome alignment and genotyping with HISAT2 and HISAT-genotype. Nat. Biotechnol. 37, 907-915.

Kind, J., and van Steensel, B. (2010). Genome-nuclear lamina interactions and gene regulation. Curr. Opin. Cell Biol. 22, 320-325.

Langmead, B., and Salzberg, S.L. (2012). Fast gapped-read alignment with Bowtie 2. Nat. Methods 9, 357-359.

Lieberman-Aiden, E., van Berkum, N.L., Williams, L., Imakaev, M., Ragoczy, T., Telling, A., Amit, I., Lajoie, B.R., Sabo, P.J., Dorschner, M.O., et al. (2009). Comprehensive mapping of long-range interactions reveals folding principles of the human genome. Science 326, 289-293.

Mamada, H., Takahashi, N., and Taira, M. (2009). Involvement of an inner nuclear membrane protein, Nemp1, in Xenopus neural development through an interaction with the chromatin protein BAF. Dev. Biol. 327, 497-507.

Margalit, A., Segura-Totten, M., Gruenbaum, Y., and Wilson, K.L. (2005). Barrier-to-autointegration factor is required to segregate and enclose chromosomes within the nuclear envelope and assemble the nuclear lamina. Proc. Natl. Acad. Sci. USA 102, 3290-3295.

Mekhail, K., and Moazed, D. (2010). The nuclear envelope in genome organization, expression and stability. Nat. Rev. Mol. Cell Biol. 11, 317-328.

Mekhail, K., Seebacher, J., Gygi, S.P., and Moazed, D. (2008). Role for perinuclear chromosome tethering in maintenance of genome stability. Nature 456,

Mikulski, P., Hohenstatt, M.L., Farrona, S., Smaczniak, C., Stahl, Y., Kalyanikrishna, Kaufmann, K., Angenent, G., and Schubert, D. (2019). The chromatin-associated protein PWO1 interacts with plant nuclear Lamin-like components to regulate nuclear size. Plant Cell 31, 1141-1154.

Misteli, T. (2007). Beyond the sequence: cellular organization of genome function. Cell 128, 787-800.

Nützmann, H.W., Doerr, D., Ramírez-Colmenero, A., Sotelo-Fonseca, J.E., Wegel, E., Di Stefano, M., Wingett, S.W., Fraser, P., Hurst, L., Fernandez-Valverde, S.L., and Osbourn, A. (2020). Active and repressed biosynthetic gene clusters have spatially distinct chromosome states. Proc. Natl. Acad. Sci. USA 117, 13800-13809.

Ptak, C., Aitchison, J.D., and Wozniak, R.W. (2014). The multifunctional nuclear pore complex: a platform for controlling gene expression. Curr. Opin.

Rao, S.S., Huntley, M.H., Durand, N.C., Stamenova, E.K., Bochkov, I.D., Robinson, J.T., Sanborn, A.L., Machol, I., Omer, A.D., Lander, E.S., and Aiden, E.L. (2014). A 3D map of the human genome at kilobase resolution reveals principles of chromatin looping. Cell 159, 1665-1680.

Reddy, K.L., Zullo, J.M., Bertolino, E., and Singh, H. (2008). Transcriptional repression mediated by repositioning of genes to the nuclear lamina. Nature 452. 243-247.

Sakamoto, Y., Sato, M., Sato, Y., Harada, A., Suzuki, T., Goto, C., Tamura, K., Toyooka, K., Kimura, H., Ohkawa, Y., et al. (2020). Subnuclear gene positioning through lamina association affects copper tolerance. Nat. Commun. 11.5914.

Schreiner, S.M., Koo, P.K., Zhao, Y., Mochrie, S.G., and King, M.C. (2015). The tethering of chromatin to the nuclear envelope supports nuclear mechanics. Nat. Commun. 6, 7159.

Servant, N., Varoquaux, N., Lajoie, B.R., Viara, E., Chen, C., Vert, J., Heard, E., Dekker, J., and Barillot, E. (2015). HiC-Pro: an optimized and flexible pipeline for Hi-C data processing. Genome Biol. 16, 1-11.

Shevelyov, Y.Y., Lavrov, S.A., Mikhaylova, L.M., Nurminsky, I.D., Kulathinal, R.J., Egorova, K.S., Rozovsky, Y.M., and Nurminsky, D.I. (2009). The B-type lamin is required for somatic repression of testis-specific gene clusters. Proc. Natl. Acad. Sci. USA 106, 3282-3287.

Shibano, T., Mamada, H., Hakuno, F., Takahashi, S.-I., and Taira, M. (2015). The inner nuclear membrane protein Nemp1 is a new type of RanGTP-binding protein in eukaryotes. PLoS One 10, e0127271.

Smith, S., Galinha, C., Desset, S., Tolmie, F., Evans, D., Tatout, C., and Graumann, K. (2015). Marker gene tethering by nucleoporins affects gene expression in plants. Nucleus 6, 471-478.

Somech, R., Shaklai, S., Geller, O., Amariglio, N., Simon, A.J., Rechavi, G., and Gal-Yam, E.N. (2005). The nuclear-envelope protein and transcriptional repressor LAP2beta interacts with HDAC3 at the nuclear periphery, and induces histone H4 deacetylation. J. Cell Sci. 118, 4017-4025.

Suzuki, R., Shindo, H., Tase, A., Kikuchi, Y., Shimizu, M., and Yamazaki, T. (2009). Solution structures and DNA binding properties of the N-terminal SAP domains of SUMO E3 ligases from Saccharomyces cerevisiae and Oryza sativa. Proteins 75, 336-347.

Tang, Y., Huang, A., and Gu, Y. (2020). Global profiling of plant nuclear membrane proteome in Arabidopsis. Nat. Plants 6, 838-847.

Towbin, B.D., Meister, P., and Gasser, S.M. (2009). The nuclear envelope-a scaffold for silencing? Curr. Opin. Genet. Dev. 19, 180-186.

Trapnell, C., Roberts, A., Goff, L., Pertea, G., Kim, D., Kelley, D.R., Pimentel, H., Salzberg, S.L., Rinn, J.L., and Pachter, L. (2012). Differential gene and transcript expression analysis of RNA-seq experiments with TopHat and Cufflinks. Nat. Protoc. 7, 562-578.

Tsatskis, Y., Rosenfeld, R., Pearson, J.D., Boswell, C., Qu, Y., Kim, K., Fabian, L., Mohammad, A., Wang, X., Robson, M.I., et al. (2020). The NEMP family supports metazoan fertility and nuclear envelope stiffness. Sci. Adv. 6, eabb4591.

Wang, Z.-P., Xing, H.-L., Dong, L., Zhang, H.-Y., Han, C.-Y., Wang, X.-C., and Chen, Q.-J. (2015). Egg cell-specific promoter-controlled CRISPR/Cas9 efficiently generates homozygous mutants for multiple target genes in Arabidopsis in a single generation. Genome Biol 16, 144.

Wolff, J., Rabbani, L., Gilsbach, R., Richard, G., Manke, T., Backofen, R., and Grüning, B.A. (2020). Galaxy HiCExplorer 3: a web server for reproducible Hi-C, capture Hi-C and single-cell Hi-C data analysis, quality control and visualization. Nucleic Acids Res 48, W177-W184.

Wong, X., Luperchio, T.R., and Reddy, K.L. (2014). NET gains and losses: the role of changing nuclear envelope proteomes in genome regulation. Curr. Opin. Cell Biol. 28, 105-120.

Xing, H.-L., Dong, L., Wang, Z.-P., Zhang, H.-Y., Han, C.-Y., Liu, B., Wang, X.-C., and Chen, Q.-J. (2014). A CRISPR/Cas9 toolkit for multiplex genome editing in plants. BMC Plant Biol 14, 327.

Xu, F., Jia, M., Li, X., Tang, Y., Jiang, K., Bao, J., and Gu, Y. (2021). Exportin-4 coordinates nuclear shuttling of TOPLESS family transcription corepressors to regulate plant immunity. Plant Cell 33, 697-713.

Yang, L., Wang, Z., and Hua, J. (2019). Measuring cell ploidy level in Arabidopsis thaliana by flow cytometry. Methods Mol. Biol. 1991, 101–106.

Zheng, R., Ghirlando, R., Lee, M.S., Mizuuchi, K., Krause, M., and Craigie, R. (2000). Barrier-to-autointegration factor (BAF) bridges DNA in a discrete, higher-order nucleoprotein complex. Proc. Natl. Acad. Sci. USA 97, 8997-9002.



#### **STAR**\***METHODS**

#### **KEY RESOURCES TABLE**

REAGENT or RESOURCE	SOURCE	IDENTIFIER
Antibodies		
anti-GFP	Takara Bio	Cat#632381; RRID:AB_2313808
anti-histone H2A	Abcam	Cat#ab18255; RRID:AB_470265
anti-HA	Roche	Cat# 11867423001; RRID:AB_390918
Goat anti-mouse IgG-HRP secondary antibody	Thermo Scientific	Cat#31430; RRID: AB_228307
Goat anti-rat IgG-HRP secondary antibody	Thermo Scientific	Cat#31470; RRID:AB_228356
Goat anti-rabbit IgG-HRP secondary antibody	Thermo Scientific	Cat#31460; RRID: AB_228341
Bacterial and virus strains		
E. coli DB3.1	N/A	N/A
E. coli DH5a	N/A	N/A
Agrobacterium tumefaciens GV3101	N/A	N/A
Chemicals, peptides, and recombinant proteins		
TRIzol Reagent	Invitrogen	Cat#15596018
Protease inhibitor cocktail	Roche	Cat#5056489001
MG132	Sigma-Aldrich	Cat#M7449
Phenylmethylsulfonyl fluoride (PMSF)	AmericanBio	Cat#AB01620-00005
DAPI	Sigma-Aldrich	Cat#D9542
Murashige & Skoog Basal Medium (MS)	PhytoTechnology Labs	Lot#14K0519111B
GFP-Trap agarose beads	Chromotek	Cat#gta-20; RRID:AB_2631357
Dynabeads <sup>™</sup> Myone <sup>™</sup> Streptavidin C1	Invitrogen	Cat#65002
Critical commercial assays		
PrimeSTAR GXL DNA Polymerase	Takara Bio	Cat# R050B
Gateway BP Clonase II Enzyme Mix	Invitrogen	Cat#11789100
Gateway LR Clonase II Enzyme Mix	Invitrogen	Cat#11791020
ClonExpress II One Step Cloning Kit	Vazyme	Cat#C112
Maxima First Strand cDNA Synthesis Kit	Thermo fisher	Cat#K1672
PowerUp™ SYBR™ Green Master Mix	Thermo fisher	Cat#A25742
Deposited data		
Raw data files for RNA-seq	This-paper	GSE147968
Raw data files for Hi-C	This-paper	PRJNA739100
Raw data files for Hi-C	(Hu et al., 2019)	PRJNA497671
Raw data files for mass spectrometry	This paper	PXD026924
Raw data files for mass spectrometry	(Huang et al., 2020)	PXD015919
Raw data files for mass spectrometry	(Tang et al., 2020)	PXD015919
The Arabidopsis thaliana genome (TAIR10)	The Arabidopsis Information Resource	http://www.arabidopsis.org
Deposited data		
Raw data for RNA-seq	this paper	GEO: GSE147968
Raw data for HiC	this paper	BioProject: PRJNA739100
Raw data for proximity labeling proteomics	this paper	ProteomeXchange: PXD026924
Experimental models: Organisms/strains		
Arabidopsis thaliana: WT; Col-0	N/A	N/A
Nicotiana benthamiana: WT	N/A	N/A
Arabidopsis thaliana: man1		N/A

(Continued on next page)





Continued			
REAGENT or RESOURCE	SOURCE	IDENTIFIER	
Arabidopsis thaliana: pnet2_a-1		N/A	
Arabidopsis thaliana: pnet2_b-1		N/A	
Arabidopsis thaliana: pnet2_b-2		N/A	
Arabidopsis thaliana: pnet2_c-1		N/A	
Arabidopsis thaliana: pnet2_c-2		N/A	
Arabidopsis thaliana: pnet2_a-1 pnet2_c-1		N/A	
Arabidopsis thaliana: pnet2_a-1 pnet2_c-2		N/A	
Arabidopsis thaliana: pnet2_b-1 pnet2_c-1		N/A	
Arabidopsis thaliana: pnet2_b-2 pnet2_c-2		N/A	
Arabidopsis thaliana: pnet2_a-1 pnet2_b-1 pnet2_c-1		N/A	
Arabidopsis thaliana: kaku4-2	(Goto et al., 2014)	N/A	
Arabidopsis thaliana: crwn1;4	(Choi et al., 2019)	N/A	
Arabidopsis thaliana: WT; 35S: PNET2_A-YFP		N/A	
Arabidopsis thaliana: WT; 35S: PNET2_B-YFP		N/A	
Arabidopsis thaliana: WT; 35S: PNET2_C-YFP		N/A	
Arabidopsis thaliana: pnet2_a-1 pnet2_b-1 pnet2_c-1; 35S: PNET2_B-YFP		N/A	
Arabidopsis thaliana: pnet2_b-2 pnet2_c-2; amiRNA-PNET2_A		N/A	
Arabidopsis thaliana: WT; 35S:MAN1-BioID2		N/A	
Arabidopsis thaliana: WT; 35S:PNET2_A-BioID2		N/A	
Arabidopsis thaliana: WT; 35S:PNET2_B-BioID2		N/A	
Arabidopsis thaliana: WT; 35S:KAKU4-BioID2		N/A	
Arabidopsis thaliana: WT; 35S:CRWN1-BioID2		N/A	
Arabidopsis thaliana: kaku4-2; NP_PNET2_B: PNET2_B-YFP		N/A	
Arabidopsis thaliana: crwn1;4; NP_PNET2_B: PNET2_B-YFP		N/A	
Oligonucleotides			
Primers for plasmid constructs, see Table S4	This paper	N/A	
Primers for genotyping, see Table S4	This paper	N/A	
Primers for qPCR assay, see Table S4	This paper	N/A	
Recombinant DNA			
35S:MAN1-BioID2		N/A	
35S:PNET2_A-BioID2		N/A	
35S:PNET2_B-BioID2		N/A	
35S:PNET2_C-BioID2		N/A	
35S:KAKU4-BioID2		N/A	
35S:CRWN1-BioID2		N/A	
35S:PNET2_A-eYFP		N/A	
35S:PNET2_B-eYFP		N/A	
35S:PNET2_C-eYFP		N/A	
NP_PNET2_B: PNET2_B-eYFP		N/A	
		N/A	
amiRNA-PNET2_A			
_		N/A	
CRISPR-PNET2_A/PNET2_C		N/A N/A	
amiRNA-PNET2_A CRISPR-PNET2_A/PNET2_C CRISPR-PNET2_B 35S:CRWN1-eYFP			
CRISPR-PNET2_A/PNET2_C CRISPR-PNET2_B 35S:CRWN1-eYFP		N/A	
CRISPR-PNET2_A/PNET2_C CRISPR-PNET2_B		N/A N/A	

(Continued on next page)



Continued		
REAGENT or RESOURCE	SOURCE	IDENTIFIER
35S:NLS-PNET2_A-C -mCherry		N/A
35S:NLS-PNET2_B-C-mCherry		N/A
35S: PNET2_A-N-NLS-mCherry		N/A
35S:PNET2_B-N-NLS-mCherry		N/A
AD-PNET2_A-N		N/A
AD-PNET2_B-N		N/A
AD-PNET2_A-C		N/A
AD-PNET2_B-C		N/A
BD-CRWN1		N/A
BD-KAKU4		N/A
BD-HTA6		N/A
BD-HTA9		N/A
BD-HTA13		N/A
BD-HTB1		N/A
BD-HTB4		N/A
BD-HTB9		N/A
35S:PNET2_B-cYFP		N/A
35S:SUN1-cYFP		N/A
35S:HTA6-nYFP		N/A
35S:HTA9-nYFP		N/A
35S:HTA13-nYFP		N/A
35S:BioID2-WIP1	(Huang et al., 2020)	N/A
Software and algorithms		
hisat2	(Kim et al., 2019)	http://daehwankimlab.github.io/hisat2/
Cuffdiff	(Trapnell et al., 2012)	http://cole-trapnell-lab.github.io/cufflinks/
agriGO	(Du et al., 2010)	http://bioinfo.cau.edu.cn/agriGO/
R version 3.4.0	The R Project for Statistical Computing,	https://cran.r-project.org/bin/windows/base/old/3.4.0/
DEP	Bioconductor	https://bioconductor.org/packages/release/ bioc/html/DEP.html
DESeq2	Bioconductor	https://bioconductor.org/packages/release/ bioc/html/DEP.html
Bowtie2	(Langmead and Salzberg, 2012)	http://bowtie-bio.sourceforge.net/
HiC-Pro	(Servant et al., 2015)	https://github.com/nservant/HiC-Pro
cworld	Job Dekker Lab	https://github.com/dekkerlab/cworld-dekker
A plasmid editor (ApE)	M. Wayne Davis	http://jorgensen.biology.utah.edu/wayned/ape/
Snapgene	Insightful Science	https://www.snapgene.com/support/downloads/
Mega-X	Molecular Evolutionary Genetics Analysis	https://www.megasoftware.net/
Zen, Black Edition	Zeiss Microscopy	https://www.zeiss.com/microscopy/int/ products/microscope-software/zen-lite.html https://www.r-project.org
GraphPad Prism v8.3.4	Informer Technologies, Inc.	http://graphpad-prism.software.informer.com/; RRID: SCR_002798
FlowJo	BD	https://www.flowjo.com/
Photoshop and Illustrator	Adobe,	http://www.adobe.com
Excel	Microsoft	N/A

**Article** 



#### **RESOURCE AVAILABILITY**

#### **Lead contact**

Further information and requests for resources and reagents should be directed to and will be fulfilled by the Lead Contact, Yangnan Gu (guyangnan@berkeley.edu).

#### **Material availability**

Materials used in this study are available from the Lead Contact upon reasonable request. This study did not generate new unique reagents.

#### Data and code availability

- Raw data files for the RNA-seq and Hi-C analysis have been deposited into the NCBI GEO: GSE147968 and BioProject: PRJNA739100, respectively, and are publicly available. Raw data files for mass spectrometry analysis have been deposited to the ProteomeXchange Database: PXD026924 and are publicly available. All MS datasets are listed in Table S5.
- This study did not generate code requiring public database deposition.
- All other data that support the findings of this study are available within the article and its supplemental information files and from the Lead Contact upon reasonable request.

#### **EXPERIMENTAL MODEL AND SUBJECT DETAILS**

#### **Plant materials**

All Arabidopsis plants used in this study are in Col-0 background. Seeds were surface-sterilized and stratified for 48 h at 4°C before growing at 22°C under a 16 h-light / 8 h-dark photoperiod. The pnet2\_a-1, pnet2\_b-1, and pnet2\_c-1 single mutants were generated in wild type (WT) Col-0 background using an egg cell-specific promoter controlled CRISPR/Cas9 system (Wang et al., 2015). The T-DNA insertion mutant SALK\_061402 (pnet2\_b-2), SALK\_029335 (pnet2\_c-2), SALK\_024888 (man1), and SALK\_076754C (kaku4) were obtained from the Arabidopsis Biological Resource Center (ABRC). The crwn1 crwn4 double mutant was obtained from Dr. Eric Richards' lab at Boyce Thompson Institute. All pnet2\_ac and pnet2\_bc double mutants were obtained from genetic crosses. The pnet2\_ab and pnet2\_abc mutants were obtained by PNET2\_B CRISPR in the pnet2\_a-1 background and PNET2\_A CRISPR in the pnet2\_b-1 pnet2 c-1 background, respectively. The pnet2 double and triple mutants were obtained by genetic crosses. The 35S: PNET2\_B-YFP transgenic lines were generated in both WT and the pnet2 triple mutant background, the 35S: PNET2\_A-YFP, 35S: PNET2\_C-YFP, 35S: PNET2\_A-BioID2, 35S: PNET2\_B-BioID2, 35S: MAN1-BioID2, 35S: CRWN1-BioID2, and 35S: KAKU4-BioID2 transgenic lines are in WT background, and the amiRNA-PNET2\_A lines are in the pnet2\_b-2 pnet2\_c-2 double mutant background. All transgenic plants were generated by floral dip transformation using Agrobacterium GV3101 carrying corresponding constructs. T1 progenies were screened on half-strength Murashige and Skoog medium (1/2 MS) supplemented with either 25 μg/mL hygromycin B (Invitrogen) or 30 μg/mL Basta (Sigma-Aldrich).

#### **METHOD DETAILS**

#### Plasmid construction

To generate CRISPR/Cas9 constructs, single guide RNAs (sgRNAs) were designed using an online bioinformatics tool (http:// crispor.tefor.net/crispor.py) and the Golden Gate method was used for cloning as described before (Xing et al., 2014). Briefly, two sgRNAs sequences that target the same PNET2 gene were incorporated into forward and reverse primers for PCR using pCBC-DT1T2 vector as the template. Purified PCR products together with the egg cell-specific promoter-driven Cas9 expressing binary vector pHEE401 were used to set up restriction-ligation reactions, resulting in the construct of pHEE401-PNET2\_A/B/C. The vector expressing amiRNA-PNET2\_A was constructed as described previously (Jia et al., 2021). A 21mer amiRNA sequence that targets PNET2\_A was designed using WDR3 online tool (http://wmd3.weigelworld.org/cgi-bin/webapp.cgi). The step-loop structured fragments were generated by overlapping PCR, and the product was inserted into Gateway entry vector pDONR207 using BP cloning (BP clonase II, Thermofisher) and subsequently cloned into destination vector pEG100 using LR cloning (LR clonase II plus, Thermofisher). For YFP or BioID2-tagged PNET2 constructs, the full-length cDNA of PNET2\_A/B/C and the full-length genomic DNA of KAKU4 and CRWN1 were inserted into a modified pEG100 vector containing YFP or BioID2 tag by In-Fusion cloning (ClonExpress II One Step Cloning Kit, Vazyme). For functional complementation assay, the construct of PNET2\_B gDNA-YFP was generated by multisite gateway cloning as described before (Gu and Innes, 2011). Similarly, the full-length cDNA of PNET2\_A/B/C, KAKU4, SUN1, HTA6, HTA7, and HTA13 were inserted into pBSDONR p1-p4, and n/c-YFP or mCherry fragments were cloned into pBSDONR p4r-p2. The pBSDONR p1-p4 and pBSDONR p4r-p2 vectors were then combined, and fusion constructs were cloned into the destination vector pEG100 using LR reaction. The truncated PNET2\_A/B C-terminal fragments were inserted into a modified pEG100 vector containing NLS-mCherry. For yeast two-hybrid assays, HTA6, HTA13 HTB1, HTB4, HTB9, KAKU4, CRWN1, and PNET2\_A/B N-/C- terminal fragments were subcloned into pGBKT7 or pGADT7 by



In-Fusion cloning. All PCR products were obtained using high-fidelity DNA polymerase (PrimeSTAR GXL, Takara), and all constructs were sequenced to ensure accuracy. All primers used for cloning are listed in Table S4.

#### Phylogenetic analysis

To construct the phylogenetic tree, PNET2 protein sequences obtained from TAIR 10 were used as the query for BLAST search (e-value < 10<sup>-4</sup>) to retrieve homologous sequences from 12 eukaryotic species, including *Populus trichocarpa*, *Medicago truncatula*, *Vitis vinifera*, *Carica papaya*, *Oryza sativa*, *Sorghum bicolor*, *Amborella trichopoda*, *Selaginella moellendorffii*, *Chlamydomonas reinhardtii*, *Physcomitrella patens*, *Drosophila melanogaster*, *Takifugu rubripes*, *Danio rerio*, *Gallus gallus*, *Mus musculus*, *Ranttus norvegiens*, *Homo sapiens*, *Pan troglodytes*, and *Xenopus tropicalis*. The plant and animal PNET2 homolog protein sequences were retrieved from Joint Genome Institute (JGI) and Ensembl databases, respectively. Multiple sequence alignment was performed using ClustalW. The phylogenetic tree of PNET2 and their homologs was generated using obtained full-length protein sequences with MEGA-X (https://www.megasoftware.net/) and the maximum-likelihood method with 1000 bootstraps.

#### **Bioinformatic analysis of PNET2s**

Transmembrane helices of PNET2s were predicted by HMMER (https://www.ebi.ac.uk/Tools/hmmer/search/phmmer). Nuclear localization signal (NLS) of PNET2s was predicted using cNLS Mapper (http://nls-mapper.iab.keio.ac.jp/cgi-bin/NLS\_Mapper\_form.cgi). Prediction of Conserved bi-helices motif was performed by Multiple Em for Motif Elicitation (MEME) (https://meme-suite.org/meme/tools/meme) and CPHmodels 3.2 Server (http://www.cbs.dtu.dk/services/CPHmodels/). Intrinsically disordered region (IDR) of full-length PNET2s was predicted by Database of Disordered Protein Predictions (D²P²) (https://d2p2.pro/) and Predictor of Natural Disordered Regions (PONDR) (http://www.pondr.com/). Normalized expression level of *PNET2s* from 79 organs and developmental stages were retrieved from RNA-seq database TraVA (Transcriptome Variation Analysis, http://travadb.org/).

#### Transient protein expression and fluorescence imaging

Agrobacterium-mediated transient protein expression in *Nicotiana benthamiana* was performed as previously described (Gu et al., 2016). For coexpression and BiFC assays, agrobacterial solution mixtures were infiltrated using a needless syringe into leaves of four-week-old *N. benthamiana* plants. About 40 h after infiltration, fluorescence images were acquired in leaf epidermal cells using a Zeiss LSM880 inverted confocal microscope. Rapid nuclear staining with DAPI was performed as described before (de Souza Junior et al., 2016). In brief, seven-day-old seedlings were fixed in fixation buffer (PBS containing 10% DMSO and 1% formaldehyde) for 30 min at room temperature and washed five times with PBS buffer, each for 10 min. Fixed seedlings were twice dehydrated with pure methanol, and four times with pure ethanol followed by washing with PBS buffer five times, each step for 10 min. Seedlings were then stained with 1 μg/mL DAPI (Thermo Fisher, Cat. #D1306) in PBS buffer for 20 min followed by washing with PBS buffer five times.

#### **Proximity-labeling proteomics and ratiometric analysis**

The BioID2-mediated and biotinylation-based in vivo proximity labeling in Arabidopsis, the subsequent label-free quantitative mass spectrometry, and ratiometric analysis have been described before (Huang et al., 2020; Xu et al., 2021). Briefly, ten-day-old transgenic seedlings expressing BioID2-tagged MAN1, PNET2\_A/B, KAKU4, and CRWN1 protein and wild-type (non-transformants, NT) were treated with 50 μM free biotin solution, and BioID2-tagged YFP transgenic lines were incubated with water. Samples were collected 24 h after treatments. Total protein was extracted with protein extraction buffer (50 mM Tris [pH 7.5], 150 mM NaCl, 0.5% Triton X-100, 0.5% Nonidet P-40, 0.5% Nadeoxycholate, plant protease inhibitor cocktail, 1 mM PMSF, and 40 mM MG132). FPLC equipped with HiTrap<sup>TM</sup> desalting column (GE Healthcare) was used to remove free biotin. The eluted protein fraction was collected and incubated with 50 μL streptavidin-coated magnetic beads (Dynabeads MyOne Streptavidin C1, Invitrogen) overnight at 4°C, and the beads were washed 5 times with protein extraction buffer. The affinity-purified samples were then boiled with loading buffer containing 50μM biotin and 1% SDS for 30 min before separated by SDS-PAGE. Protein gels were stained with Coomassie blue R-250, cut into three gel pieces for each lane, and digested with trypsin in 50 mM ammonium bicarbonate at 37°C overnight. The peptides were extracted twice with 1% formic acid in 50% acetonitrile aqueous solution and dried by Speedvac before LC-MS/MS analysis was performed. To identify enriched protein candidates, ratiometric analysis was performed with peptide peak areas (LFQ values) as input using DEP package in R. Candidates with normalized peptide spectrum match value bigger than 0.5 (PSM > 0.5) were further filtered by cutoffs fold-change > 2 and p-value < 0.1 compared with both controls. Gene Ontology (GO) enrichment analysis was performed using the DAVID Bioinformatics Resources (https://david.ncifcrf.gov/).

#### RNA-seq and data analysis

Total RNA was purified from 7-day-old seedlings using RNAprep pure Plant Kit (TIANGEN, DP432). Libraries for RNA-seq were generated using the NEBNext® Ultra Directional RNA Library Prep Kit for Illumina. Briefly, RNAs were enriched and fragmented using RNA fragmentation buffer. Fragmented RNAs were used for the first and second-strand cDNA synthesis. Double-stranded cDNAs were purified, end-repaired, and ligated to adapters. Ligated products were amplified for 12-15 cycles, and the PCR library was purified using Agencourt AMPure XP beads. The libraries were subjected to Illumina PE150 sequencing by Novogene (Beijing). Sequencing read counts were trimmed and quality filtered to clean reads. Cleaned reads were mapped to the Arabidopsis reference genome (TAIR10) using Hisat2. Cuffdiff was used for calculating gene expression levels (normalized for TMP, Transcripts Per Kilobase of exon model per Million mapped reads). DESeq2 package in R was used to identify differentially expressed genes

Article



(DEGs) under the criteria of adjusted p-value < 0.01 and fold change > 2 or < 0.5. GO analysis was performed by AgriGO V2.0 (http:// systemsbiology.cau.edu.cn/agriGOv2/).

#### RT-qPCR

For real-time qPCR, total RNA was extracted from 4-day-old seedlings using TRIzol reagent (Invitrogen, Cat. # 15596026). Removal of integrated DNA and synthesis of the first-strand cDNA was performed using a Maxima First Strand cDNA Synthesis Kit with dsDNase (Thermo Scientific, Cat. # K1672). RT-qPCR was performed on a CFX96TM Real-Time System (Bio-Rad) using SYBR Green PCR Master Mix (Thermo Fisher, Cat. # 4309155). ACTIN2 (AT3G18780) was used as the reference gene and Student's t-tests were performed using two biological replicates for each sample. Statistical analysis was performed using Prism GraphPad (v8.3.4).

#### Yeast two-hybrid assay

Yeast two-hybrid analysis was performed according to the manufacturer's protocol (Clontech, MATCHMAKER GAL4 Two-Hybrid System). Two combinatory constructs were cloned into bait vector pGBKT7 and prey vector pGADT7 before transformed into the yeast strain AH109 and Y187, respectively. The transformed cells of AH109 and Y187 expressing corresponding constructs were mated in 200 μL 2× YPDA medium at 30 °C for 20-24h. The diploid yeasts were cultured and selected on double (SD-Leu-Trp), triple (SD-Leu-Trp-His), and quadruple (SD-Leu-Trp-Ade-His) synthetic dropout medium at 30 °C for 3-5 days.

#### **Co-immunoprecipitation**

PNET2\_A-YFP was transiently expressed in N. benthamiana leaves. Total protein was extracted with protein extraction buffer (50 mM Tris-HCI [pH 7.5], 150 mM NaCl, 0.5% Triton-X 100, 0.5% NP-40, 0.5% sodium deoxycholate, 1 mM PMSF, 40 μM MG132, and protease inhibitor cocktail). For immunoprecipitation, the total protein extract was incubated with 20 µl GFP-Trap agarose beads (Chromotek gta-20) overnight at 4°C. The beads were washed five times with protein extraction buffer. The immunoprecipitated proteins were eluted by boiling with SDS loading buffer for 15 min at 95°C and separated by SDS-PAGE before being immunoblotted with anti-GFP antibody (Clontech, #632381) and anti-histone H2A antibody (Abcam, ab18255), respectively.

#### Flow cytometry of cell ploidy level

The ploidy levels of cotyledon were performed as previously described (Yang et al., 2019). Briefly, 0.25 mg cotyledon of 10-day-seedlings were immersed in 600 μL Aru buffer (1mM MgSO4, 15mM KCl, 5mM HEPES, 1 mg/mL dithiothreitol, 0.0025% Triton X-100, 100 mg/mL PI, 100 mg/mL RNase A) chopped with a new razor blade to release the nuclei. The resulting homogenate were filtered by a 40 µm cell strainer and incubated on ice for 30 min. The DNA content of cotyledon cell nuclei were determined by a Becton Dickinson LSR-II flow cytometer with a blue laser (100 mW 488 nm). For each genotype, two biological replicates were prepared and about 10000 flow cytometric events were recorded. The output was gated to remove the signal from cell debris and chloroplast. Data analysis was performed by FlowJo software (https://www.flowjo.com/solutions/flowjo).

#### HiC and data analysis

Hi-C libraries of 7-day-old WT and pnet2\_abc seedlings were constructed according to the protocol published previously (Dong et al., 2018). Subsequent sequencing was completed by Illumina HiSeq X Ten instrument (PE 100bp mode). Low-quality reads and adapters were filtered and removed before sequencing reads were mapped to the Arabidopsis thaliana genome (TAIR 10, https://www.arabidopsis.org) by bowtie2. Then, self-ligated, dangled, and invalid read pairs were identified and discarded. The remaining ~332 million and ~392 million valid read pairs in WT and the pnet2\_abc mutant, respectively, were retained for construction of the interaction map. Hi-C interaction matrices enclosing paired equal-sized bins at various resolutions were calculated using Hi-C-Pro and visualized by hicPlotMatrix. The resolution of Hi-C interaction map was evaluated based on the previous definition (Grob et al., 2013; Rao et al., 2014). To compare the difference of chromatin interactions between WT and pnet2\_abc mutant, respective Hi-C contact matrices were trimmed to the same sequencing depth by hicNormalize. The differential chromatin interaction matrix was generated by hicCompareMatrices. Genome-wide chromatin loops were identified using Fit-Hi-C at the 1 kb resolution (default settings) (Ay et al., 2014). Here, the 1kb resolution is calculated as the minimal interval between the starting coordinates of two looppaired bins. Identifications of IHIs (Interactive Heterochromatic Islands) or KEEs (KNOT ENGAGED ELEMENTs) were completed at the 100 kb resolution following the published method (Feng et al., 2014; Grob et al., 2014). Exemplary interleaved interaction web among different IHI/KEEs were generated using HiCExplorer (Wolff et al., 2020). The interaction frequency decay dependent on the genome distance was evaluated by IDE (Interaction Decay Exponents), which was defined as the slope of linear fit to the decreased contacts with increased genomic distance (Grob et al., 2014; Lieberman-Aiden et al., 2009). In this study, IDE values for genomic distances ranging from 100kb to 10 Mb were calculated. Using the matrix2compartment module in cworld (https:// github.com/dekkerlab/cworld-dekker), compartments within WT and pnet2\_abc mutant were determined by characterizing and comparing the first-dimension PCA (principal component analysis) components (PC1) of the chromatin interaction matrix within each chromosome. The group of regions with high gene density and positive PC1 values was defined as A compartment group, while the group of regions exhibiting contrast PC1 values was defined as B compartment group. Respective A-to-B and B-to-A compartment switches were specifically characterized for each 100kb compartmentalized bin.